



**Politecnico
di Torino**

Corso di Laurea Magistrale in Ingegneria Elettronica

Tesi di Laurea Magistrale

**Study and investigation of Active
EMI filtering techniques able to
minimize conducted
electromagnetic emission on
DC/DC converters**

Relatori:
Prof. Gianluca SETTI
Ing. Davide LENA

Candidato:
Silvia SIMONE

October 2022

Summary

As electronic systems get more sophisticated, strongly heterogeneous functional blocks are required to be placed close to each other in a strictly constrained amount of space (either at board level, system-on-a-chip level, or integrated level) to fulfil the reduced requirements on the size and the costs of the desired final solution. The coexistence of such different functional blocks leads to many circuitual issues. Here, the problem of electromagnetic interference (EMI) generated by a circuit and affecting nearby ones is considered. The relevance of this problem is such that, in the design of any circuit, it is mandatory to comply with a set of international regulations that limits the level of the emitted electromagnetic energy to ensure the electromagnetic compatibility (EMC) of the device with ones located in the nearby environment.

Over the years, several techniques have been developed with the aim of complying with these regulations. Focusing on the conducted emission regulatory requirements (which refer to the electromagnetic energy that propagates by a direct conduction on metallic conductors' paths), a possible solution consists in introducing EMI passive filters whose components' values depend on the desired attenuation that allows to reduce the emission to the desired level.

Of course, the introduction of additional EMI filters to the overall system is not cost-free at all, as it leads to a significant increase both in price and in board area. Therefore, an innovative and recently developed technique consists in exploiting active filters, whose working principle is remarkably analogous to the active noise control method.

The working principle consists in evaluating the unwanted interference signal and simultaneously injecting an antiphase copy of it, with the aim of completely cancelling it out or, at least, reducing it. This allows to achieve the same attenuation levels with respect to the passive solution, with a smaller volume and costs, thanks to the reduced size of the components employed and the low impact that parasitic resistors have on the active filter attenuation.

In this thesis work, in collaboration with STMicroelectronics, the implementation of an active filter device for a prototype of a step-down DC/DC constant

on-time power converter provided by STMicroelectronics has been investigated. The converter belongs to the class of switch mode power supply (SMPS), where the high switch voltage and fast current slew rates that occur during switching transitions cause it to be a major source of EMI.

After having analysed the setup environment for evaluating the conducted emission, an equivalent model for performing the simulation is implemented and the device's conducted emission level are studied by means of the SIMPLIS © simulation environment. An active EMI filter has been designed, also exploiting MATLAB © in the preliminary phases. The design phase has been tackled taking into account the required emission levels that must be respected to comply with the regulatory requirements. The active topology impact on the overall system's performances has been hence evaluated, and a direct comparison with respect to some typical passive topologies has been performed.

The proposed solution highlights a non-negligible reduction in terms of total occupied area and costs, guaranteeing at the same time a satisfactory attenuation level of the conducted emitted disturbances.

Table of Contents

Acronyms	3
1 Electromagnetic Compatibility	6
1.1 Introduction on the EMC	6
1.2 Conducted interference	8
1.2.1 Standard regulation	11
1.2.2 Line Impedance Stabilization Network	13
1.2.3 EMI Receiver	15
1.3 Radiated interference	17
1.3.1 Radiation effects of DM and CM currents	18
2 Simulation of conducted emissions	23
2.1 EUT	23
2.1.1 EUT configuration	26
2.2 LISN configuration	28
2.3 Test receiver configuration	31
3 Design of input filter	36
3.1 Specification analysis	36
3.2 Impact on stability	38
3.3 Impact on performance	41
4 Passive filter	47
4.1 LC filter	47
4.1.1 Damping	51
4.1.2 Filter components final values	57
4.2 π -filter	60
4.3 Comparison between LC and π filter	65

Table of Contents

5 Active filter	68
5.1 Active filter topologies	68
5.2 Active filter design	70
5.3 Comparison between AEF and π -filter	84
6 Conclusions	91
Bibliography	95

Acronyms

AEF

active EMI filter;

AM

artificial network: network that provides a defined impedance to the EUT, couples the disturbance voltage to the measuring receiver, and decouples the test circuit from the mains network or other power lines [1];

AMN

artificial main network: network that provides a defined impedance to the EUT, couples the disturbance voltage to the measuring receiver, and decouples the test circuit from the supply mains [1];

CM current

common mode current: vector sum of the currents flowing through two or more conductors at a specified cross section of a "mathematical " plane intersected by these conductors [1];

CM voltage

common mode voltage also called asymmetric voltage: RF voltage appearing between the electrical mid-point of the individual terminals or leads in a two or multi wire circuit and reference ground [1];

DM current

differential mode current: half the vector difference of the currents flowing in any two of a specified set of active conductors at a specified cross-section of a "mathematical " plane intersected by these conductors [1];

DM voltage

differential mode voltage also called symmetric voltage: RF voltage appearing between any pair of wires not comprising the wire at ground potential in a two or multi wire circuit, such as a single-phase mains supply or a bundle of twisted pairs in a communication cable [1];

EMC

electromagnetic compatibility;

EMI

electromagnetic interference;

EUT

equipment under test: equipment (devices, appliances and systems) subjected to EMC (emission) compliance tests [1];

LISN

line impedance stabilization network: AMN which couples unsymmetric voltages [1];

TR

test receiver: instrument such as a tunable voltmeter, an EMI receiver, a spectrum analyzer or an FFT based measuring instrument, with or without preselection, that meets the relevant clauses of CISPR 16-1-1 [1].

Chapter 1

Electromagnetic Compatibility

1.1 Introduction on the EMC

The enormous use of electronic equipment in recent decades has made it necessary to take into consideration several aspects that go beyond the normal functionality of these devices in the design process. As a matter of fact, the related electromagnetic phenomena hardly remain confined within such equipment during their normal operation, propagating through conductors and free space and potentially affecting the behavior of other electronic systems. Evolution of technologies have made the various electronic systems smaller, more sophisticated and with a lower power consumption, leading, on the other hand, to a greater sensitivity to disturbances coming from the outside of the device. To solve these problems, an engineering field of application called Electromagnetic Compatibility (EMC) was born. Electromagnetic Compatibility is defined as the ability of an electronic device to work properly in the environment in which it is inserted, without producing or be susceptible to interference. The produced interference are the conducted or radiated electromagnetic emissions that must be of an extent as not to pollute the surrounding electromagnetic environment beyond well defined limits. Susceptibility is a measure of the ability of an apparatus to receive unwanted signals, and therefore to be disturbed. Conversely, immunity represents the ability of the devices to remain protected from these interference.

An apparatus is Electromagnetically Compatible with its environment if the following three requirements are met:

1. it does not cause interference with other systems close to it;
2. it is not susceptible to emissions generated by other systems
3. it does not cause interference with itself.

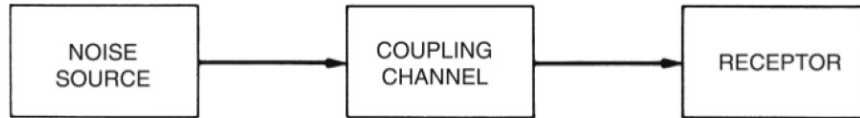


Figure 1.1: Main elements of the EMC coupling problem.

EMC deals with generation, transmission and reception of electromagnetic energy, hence EMC problems to exist need:

- a system or a device that generates interference, that is the culprit;
- a coupling path, that can be power lines or signal lines in case of conducted phenomena and magnetic, electric, or plane wave in case of radiated phenomena;
- a system or a device that is susceptible to the interference, that is the victim.

These three different elements suggest three possible solutions to act on: suppress emission at the source, make the coupling channel inefficient, make the receiver less susceptible to interference.

To regulate and standardize the electromagnetic compatibility rules in all countries, directives have been issued. In the US, the *Federal Communications Commission* (FCC) is the government agency that imposes requirements on the placement of electrical products on the market, whereas European standards are regulated by the *Comité International Spécial des Perturbations Radioélectriques* (CISPR), which is part of the *International Electrotechnical Commission* (IEC). *Mutual recognition agreements* (MRA) exploit EMC testing to cover wider geographical or market areas. In the case of conducted emissions, FCC and CISPR limits are the same. Any electrical or electronic device, to be placed on the market, must comply with one or more harmonised standards. To ensure

compliance with these regulations, it is responsibility of the manufacturer or an organization certified to provide a declaration of conformity.

The EMC problem must be addressed from the design stage, hence it is important to carry out some considerations on:

- *product cost*: if no action is taken until quality control is reached, it's very difficult for the apparatus to automatically comply with the standards and the designers have to intervene with more expensive solutions;
- *product marketability*: considering the product appearance and its usability, for example confining a typewriter in a metal box to reduce radiated emissions would make it unusable for the consumer;
- *manufacturability of the product*: any components added to suppress EMC disturbances must be easily manageable in the production process;
- *product development schedule*: the product must be placed on the market within a certain period of time to exploit the interest of the consumer. Any development delay affects the product's marketability, leading to a loss of profits for the manufacturer.

1.2 Conducted interference

In the case of conducted coupling, the interference propagates through conductor cables that connect different parts of a circuit or different circuits to each other. These cables can be power cables, data transmission cables, interconnection cables between devices, etc. and conduct emission or conduct susceptibility problems may occur.

● Conducted Emissions

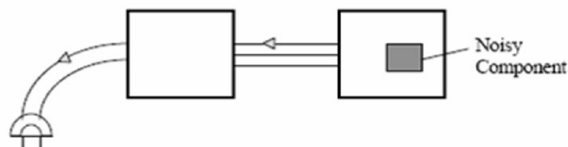


Figure 1.2: Conducted emissions EMC problem.

● Conducted Susceptibility (Immunity)

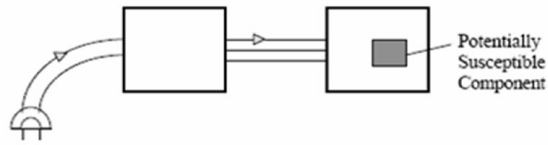


Figure 1.3: Conducted susceptibility EMC problem.

This section focuses mainly on the problem of conducted emission as they will be the main ones to consider for the design of the EMC filter. Conducted emissions (CE) refers to the mechanism which allows to generate electromagnetic energy in an electronic device and coupled to its AC power cord. The commercial power distribution system in a structure is a wide range of wires connecting the various power outlets from which the other electronic systems in the installation receive their ac power, electromagnetic energy that is coupled to a product's power cord can find its way to the entire power distribution network and use the larger network to radiate more efficiently than the product could by itself, therefore the conducted emissions may cause radiated emission, which may then cause interference.

Differential Mode (DM) and Common Mode (CM) signals represent two forms of conducted emissions. DM currents are generally referred to as symmetrical mode signals or transverse signals, whereas CM currents are also known as asymmetrical mode or longitudinal signals. In Figure 1.4 there is a representation of DM and CM current paths in a synchronous buck converter, the capacitors C_{Y1} and C_{Y2} connected from positive and negative supply lines to earth ground are inserted to represent the common mode current propagation path.

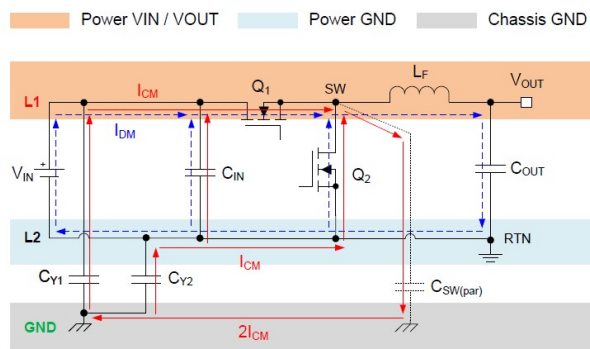


Figure 1.4: DM and CM conducted noise paths for a buck converter [2].

The DM current is due to the inherent switching of the converter and it flows in opposite directions in the positive and return power lines, using one of the two conductors as a forward path and the other for the return. DM noise generally flows in a small loop area, with a close and compact return path. A buck converter operating in continuous conduction mode (CCM) draws a trapezoidal-shaped current with harmonics that occur as noise on power lines. The input capacitor of the buck converter helps to compensate these higher order current harmonics, but some harmonics inevitably are present in the supply current as DM noise. The differential mode current path for a synchronous buck converter is represented in blue in Figure 1.4.

Instead, the CM current propagates in the same direction on both conductors using the metal case as a return line through the parasitic capacitors present between the conductors and the case itself: the current flows in the earth GND wire and returns via power lines. In the case of a non isolated dc-dc switching converter, the CM noise is mainly due to the high dv/dt at the switching node (SW) causing a displacement current that couples to the GND through the MOSFET's parasitic capacitance or the coupling capacitance associated with long cables from converter's input or output, representing a CM noise path. The common mode current path is represented in red in Figure 1.4. This current typically flows in a large conducting loop area, acting like an antenna and representing a possible cause of radiated EMI increase.

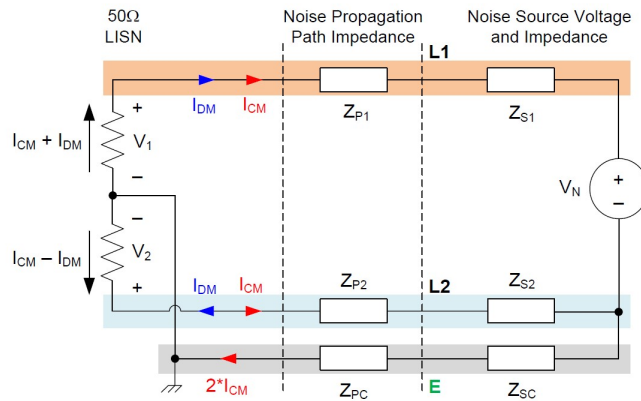


Figure 1.5: Conducted EMI model for a dc-dc converter with noise source, noise propagation path and LISN equivalent circuit.

In Figure 1.5 the noise source is represented as V_N , the noise source impedance is denoted as Z_S and propagation path impedance is indicated as Z_P , while

the high frequency equivalent circuit of the instrument used for the conducted emissions test is depicted with two 50Ω resistors. Relations for DM and CM components can be expressed as:

$$|V_{total}| = |V_1| = |50 \cdot (I_{CM} + I_{DM})| \quad (1.1)$$

$$|V_{total}| = |V_2| = |50 \cdot (I_{CM} - I_{DM})| \quad (1.2)$$

$$\text{DM noise voltage} \rightarrow |V_{DM}| = \left| \frac{V_1 - V_2}{2} \right| = |50 \cdot (I_{DM})| \quad (1.3)$$

$$\text{CM noise voltage} \rightarrow |V_{CM}| = \left| \frac{V_1 + V_2}{2} \right| = |50 \cdot (I_{CM})| \quad (1.4)$$

1.2.1 Standard regulation

The allowable conducted emissions from electronic devices are controlled by regulatory agencies and the limits refer to different standards according to the sector of application (Figure 1.6).

Product sector	CISPR standard	EN standard	FCC standard
Automotive	CISPR 25	EN 55025	–
Multimedia	CISPR 32	EN 55032	Part 15
ISM	CISPR 11	EN 55011	Part 18
Household appliances, electric tools and similar apparatus	CISPR 14-1	EN 55014-1	–
Lighting equipment	CISPR 15	EN 55015	Part 15/18

Figure 1.6: Summary of main product standards for conducted emissions [3].

- The EMI standards for automotive components and modules are specified in CISPR 25 [4], measurements are performed using one or two $5\mu H/50\Omega$ Artificial Networks (ANs) depending on the grounding configuration. Class 5 is the most stringent (Figure 1.7) and this test covers 150 kHz to 108 MHz in specific frequency bands (AM and FM radio, and mobile service bands).

32, while for Class A the limits depend on the equipment group and power level (Figure 1.9).

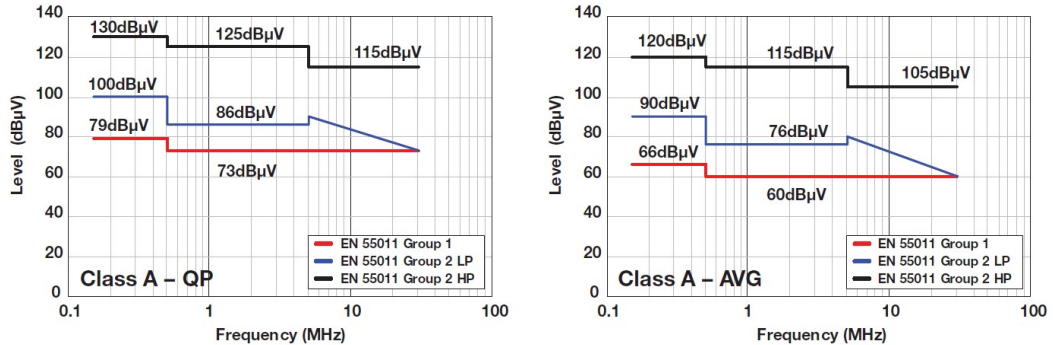


Figure 1.9: CISPR 11 Class A conducted emission limits.

1.2.2 Line Impedance Stabilization Network

The measurement procedure that is used to verify compliance with the conducted emission regulatory requires an artificial main network that is the line impedance stabilization network - LISN/AMN - placed between the input power supply and the EUT and a spectrum analyzer, which is attached to the LISN and measures the conducted emissions of the product.

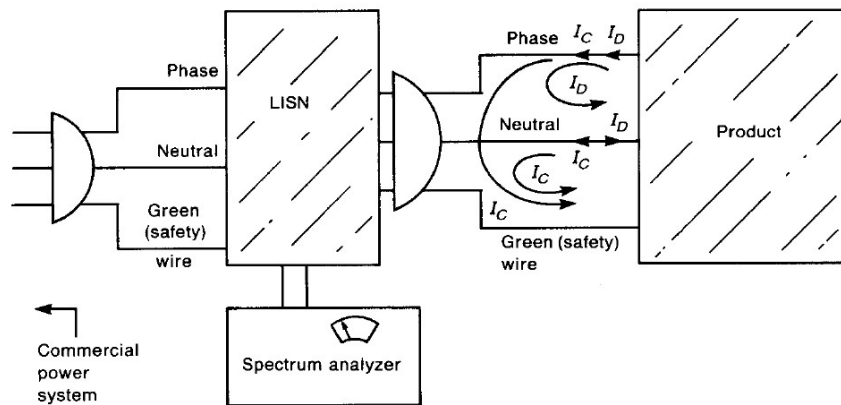


Figure 1.10: Use of a LISN in the measurement of conducted emissions.

The purpose of the conducted emission test is to measure the noise currents that exit the product's power cord conductors. However, it is necessary to be able to compare all the measurements, even if they are made in different places and times. Therefore, testing with a current probe is not admitted at all, due to the variability of the load connected to the equipment under test, which influences the intensity of the disturbances conducted on the power supply cable. This load, namely the impedance seen by the device looking into the power system, varies considerably over the measurement frequency range from site to site. For these reasons a LISN is required which is a device capable of meeting the following characteristics:

- to present a constant impedance between the product's power conductor over the frequency range of the conducted emission test,
- to block conducted emissions that are not due to the product testing and avoid external noises conducted on the electrical network can alter the measurement,
- to create a decoupling between the load and the network so that any disturbances in the load do not affect the network,
- to let the supply current circulate whether it is alternating at 50 Hz or continuous.

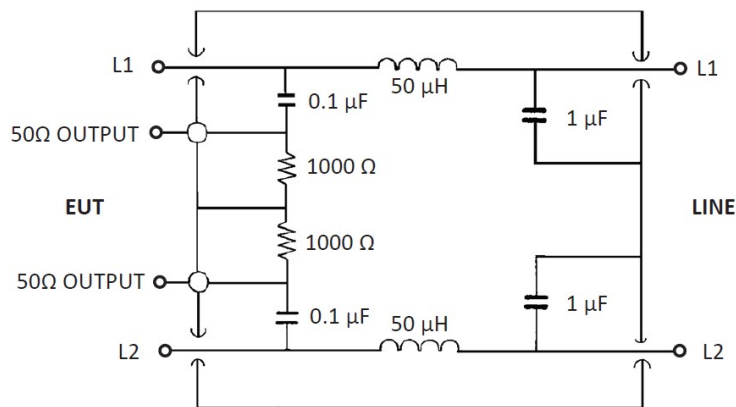


Figure 1.11: Typical $50 \mu H$ LISN used for CISPR 32 conducted emissions measurements.

The $1 \mu F$ capacitance and the $50 \mu H$ inductor have the task of preventing the disturbance present on the energy distribution network from crossing the

measuring device, leading to a test result falsification. The capacitance of $0.1 \mu F$ must prevent any dc current overload on the receiver input. Computing the impedances of these elements at the boundary of regulatory limit 150 kHz and 30 MHz the capacitors are low impedances over the measurement frequency range, and the inductor presents a large impedance:

Element	$Z_{150\text{kHz}}$	$Z_{30\text{MHz}}$
50 μH	47.1 Ω	9424.8 Ω
0.1 μF	10.61 Ω	0.053 Ω
1 μF	1.06 Ω	0.0053 Ω

When the measurement is performed, resistances of 50 Ω are placed in parallel with the $1k\Omega$ resistors: one 50 Ω resistor is the input impedance of the spectrum analyzer, while the other port must be in any case closed with a 50 Ω resistor to ensure that the impedance between phase and the green wire and between neutral and the green wire is approximately 50 Ω for all the time.

1.2.3 EMI Receiver

The EMI receiver is the instrument which permits to measure conducted disturbances. It behaves as a spectrum analyzer: it is in fact a superheterodyne receiver, with the additional ability to provide the quasi-peak computation, as well as the peak value. This is very useful in the conducted emissions measurement, as the limits provide the maximum quasi-peak and average value, allowing therefore a direct comparison with the the measured values.

The super heterodyne receiver is composed by a variable local oscillator, a narrow band amplifier focused on a particular frequency and by a mixer as can be seen in Figure 1.12. The input signal and the signal from the oscillator arrive at the mixer, thus the output signal is the result of the product of the input frequencies. When the output signal will be concentrated on the amplifier band, it will be possible to carry out the measurement and display it on the screen. Since the local oscillator varies its frequency it's possible to cover the entire range of values of interest involved for the measure and thus obtain the desired detection.

The receiver is also equipped with an input stage consisting of a selector filter and a low-noise preamplifier. The presence of the attenuator at the input of the chain avoids the saturation of the most sensitive receiver stages, however

it may happen that low intensity signals are not measurable because they cannot be compared with the background noise. The use of the pre-selector filter, composed of a set of band pass filters with different central frequency, in conjunction with the attenuator, allows the measurement of a wide range of values of the input signals, obtaining information on signals with very different amplitudes.

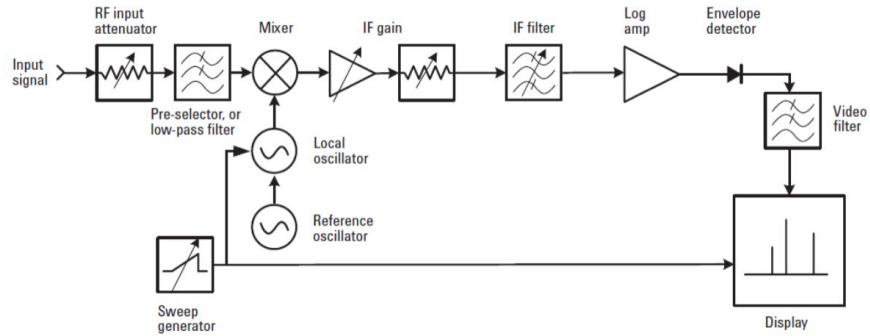


Figure 1.12: Block diagram of EMI receiver.

1.3 Radiated interference

Radiated emission refers to the generation of disturbance that propagate through the environment, instead radiated susceptibility concerns the system that is victim of that interference.

● Radiated Emissions

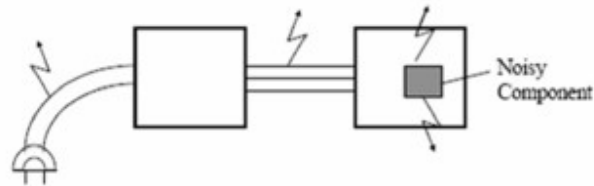


Figure 1.13: Radiated emissions EMC problem.

● Radiated Susceptibility (Immunity)

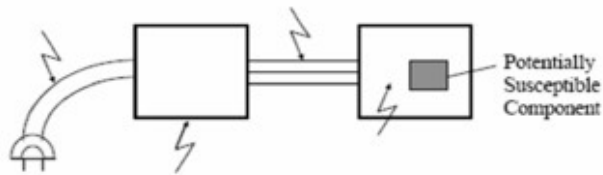


Figure 1.14: Radiated susceptibility EMC problem.

The tests for radiated emission extend to a frequency of 1GHz and they are performed either in an open-area test site (OATS) or in a semianechoic chamber (SAC): it is a shielded room with radio-frequency absorber material on its walls, preventing both reflections (hence simulating free space) and a measurement alteration due to electromagnetic emissions from the external environment. A biconical, log-periodic or a horn antenna is used, depending on the range of frequency of the test. An example of the measurement setup can be seen in Figure 1.15.

Instead, the purpose of the tests performed to verify radiated susceptibility is to ensure that the product works correctly when it is installed near high power transmitters, the commonly used ones are airport surveillance radars and AM and FM transmitters. Devices are tested by being illuminated with a waveform

and a signal level equal to the worst exposure of the product to check if it will continue to function properly.

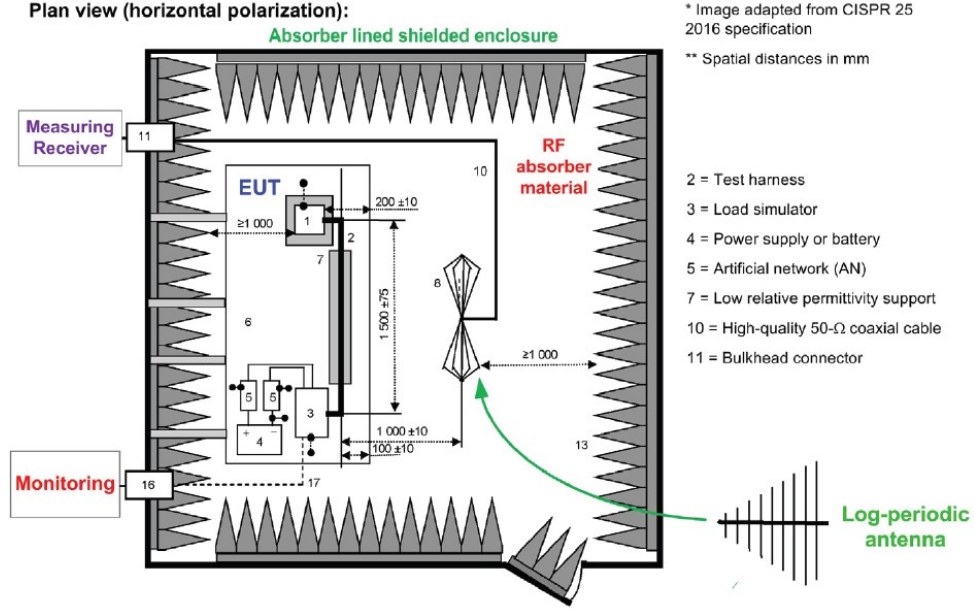


Figure 1.15: CISPR 25 radiated emissions measurement setup with biconical antenna (30MHz to 300MHz) or log-periodic antenna (200MHz to 1GHz) [7].

1.3.1 Radiation effects of DM and CM currents

The DM current and CM current flow in a large conducting loop area, act as an antenna and represent a possible mechanism for increasing radiated disturbance, therefore reducing conducted emissions helps in mitigate also radiated emissions. The radiated fields can be determined, under the assumption of constant current distributions, for electrically short segments of current, so as to hypothesize that at any point of the antenna the intensity and phase of the current are equal, by considering each wire as a Hertzian dipole:

$$(\text{Hertzian dipoles}) \begin{cases} \hat{M} = j \frac{\eta_0 \beta_0}{4\pi} \mathcal{L} = j 2\pi \times 10^{-7} f \mathcal{L} \\ F(\theta) = \sin\theta \end{cases} \quad (1.5)$$

Considering a pair of parallel conductors the total radiated electric field is the superimposition of the radiated fields of each conductor:

$$\hat{E}_\theta = \hat{E}_{\theta,1} + \hat{E}_{\theta,2} \quad (1.6)$$

$$\hat{E}_\theta = \hat{M} \frac{e^{-j\beta_0 r}}{r} \left(\hat{I}_1 e^{+j\beta_0 s/2\cos\phi} + \hat{I}_2 e^{-j\beta_0 s/2\cos\phi} \right) \quad (1.7)$$

- for DM :

the differential mode currents \hat{I}_D that are the wanted currents, have the same magnitude but opposite direction:

$$\hat{I}_1 = \hat{I}_D \quad (1.8)$$

$$\hat{I}_2 = -\hat{I}_D \quad (1.9)$$

substituting these values in the expression of the radiated field, considering $\frac{1}{2}\beta_0 s = \pi s/\lambda_0 = \pi s f/v_0 = 1.05 \times 10^{-8} s f$, and assuming the value s of the wire spacing electrically small in order to approximate $\sin(\frac{1}{2}\beta s) \approx \frac{1}{2}\beta s$, the final electric field for DM is:

$$\left| \hat{E}_{D,max} \right| = 1.316 \times 10^{-14} \frac{|\hat{I}_D| f^2 \mathcal{L} s}{d} \quad (1.10)$$

Considering a trapezoidal waveform, that is the case of the input current of a buck converter the spectra obtained are the following:

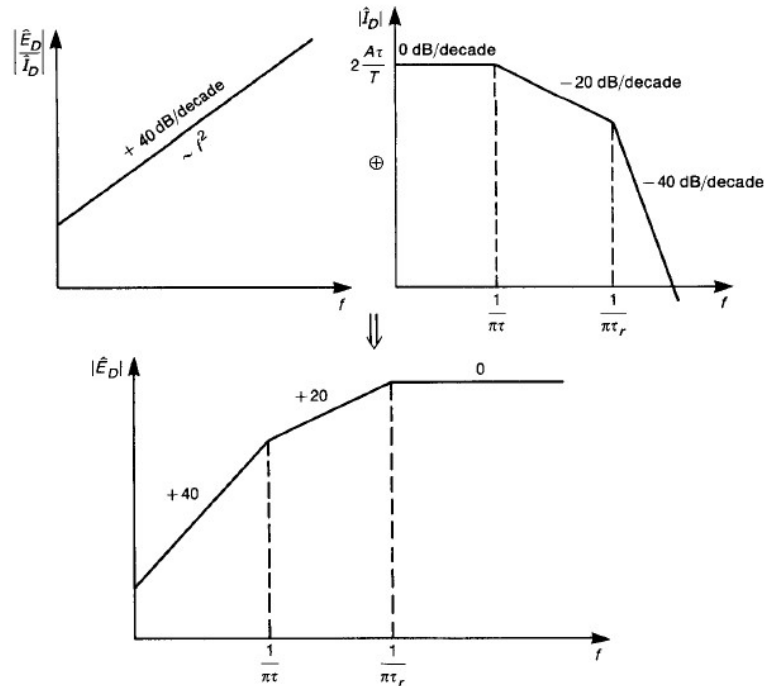


Figure 1.16: Spectral content of the radiated emission due to the DM currents.

consequently using a filter to reduce the DM current also reduce the radiated field. At a given frequency, the contrivance to reduce the radiated emission caused by the differential mode current are: reducing the current level, and reducing the loop area, since the electric field depend on the *loop area* $A = \mathcal{L}s$;

- for CM:

the common-mode currents, that are the undesired currents, have the same magnitude, but are oriented in the same direction:

$$\hat{I}_1 = \hat{I}_C \quad (1.11)$$

$$\hat{I}_2 = \hat{I}_C \quad (1.12)$$

therefore the final electric field obtained superimposing the fields of the two Hertzian dipoles in this case is:

$$|\hat{E}_{C,max}| = 1.257 \times 10^{-6} \frac{|\hat{I}_C| f \mathcal{L}}{d} \quad (1.13)$$

and the spectra of the radiated emissions due to the CM currents for a trapezoidal pulse train, are the following:

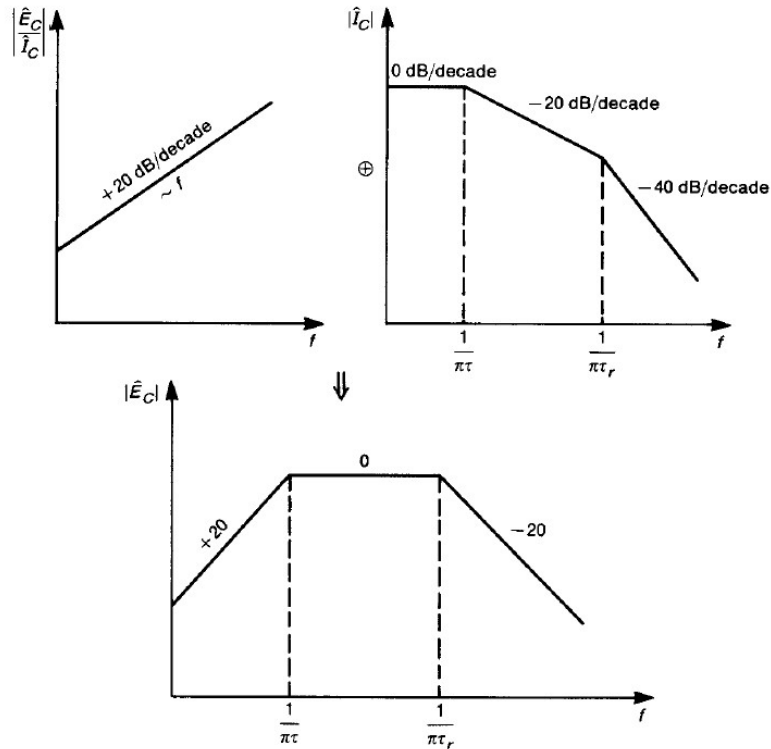


Figure 1.17: Spectral content of the radiated emission due to the CM currents.

in this situation, since the electric field is proportional to the amplitude of the CM current and to the line length, for reducing the electric field it is necessary either to act on the common mode current, reducing the overall current level, or reducing the line length \mathcal{L} .

Another possible solution consists in either increasing the pulse rise or fall times or reducing the pulse train frequency, shifting at a lower frequency the two breakpoints $\frac{1}{\pi\tau}$, $\frac{1}{\pi\tau_r}$ in the spectrum of radiated emission, anticipating the frequency range where the spectrum is characterized by a -20 dB/dec slope.

Chapter 2

Simulation of conducted emissions

This chapter illustrates the equipment under test (EUT) where the study of conducted emissions is conducted as described in [8], [9], [10] and for the subsequent realization of an EMC filter, making it compliant with standard requirements. The instruments' model used to carry out conducted emissions tests are presented as detailed in [11] in order to have a reliable simulation environment.

2.1 EUT

The device under analysis is a buck regulator (Figure 2.1), that is a step down converter belonging to the class of the Switched-Mode Power Supply (SMPS). Nowadays, SMPS are more and more widespread at the expense of linear supplies, due to their higher efficiency, in fact for a linear supplies typically the efficiency is of the order of 20–40%, instead for SMPS it reaches the order of 60-90%. Furthermore SMPS also tend to have a lighter weight than linear power supplies, due to the fact that the first have transformers lighter in weight than those of the latter.

In this case the switching element is the MOSFET, that gets in input on the gate a square-wave pulse train with a pulse width t and a frequency $f = 1/T$, that turns the MOSFET on and off and this action generates a pulsed voltage of the same duty-cycle at V_{in} . The average value of the pulsed waveform can be changed varying the duty cycle of the switching signal applied to the gate of the MOSFET, therefore changing the duty cycle the output voltage is regulated. The

inductor L and the capacitance C constitute a low pass filter that lets pass the dc component of the waveform, instead the diode provides a discharge path when the transistor is turned off.

Another advantage of switching regulator is that the MOSFET is either turned full on or full off, dissipating much less power than linear one, where the switch element is always operating in linear region generating greater dissipation.

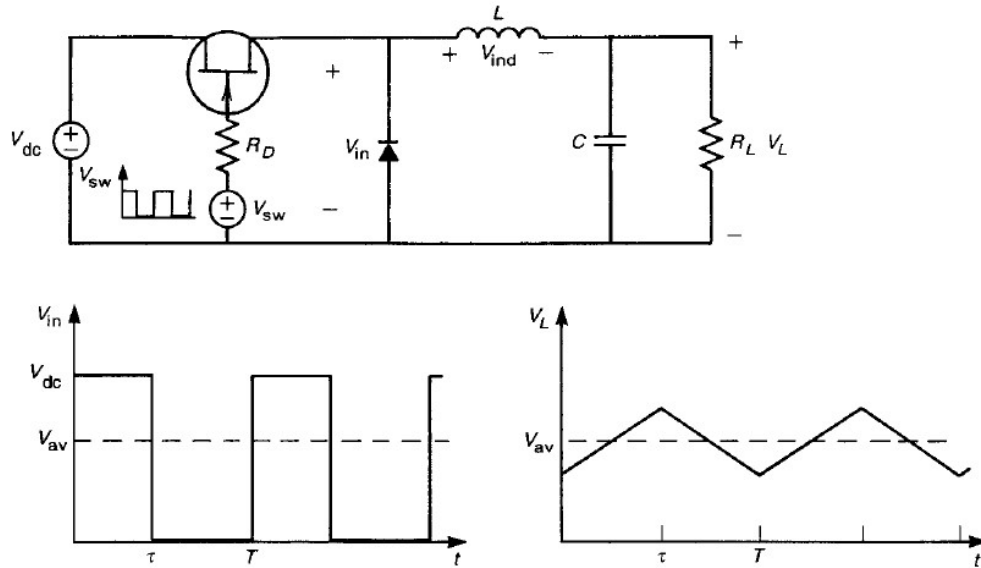


Figure 2.1: Buck regulator switching power supply.

A possible control technique used for buck converters is the constant on-time mode. This approach utilizes the output ripple as a ramp signal comparing it with a reference voltage, and if it is lower than V_{ref} , the signal that drives the transistors is enabled for a fixed time T_{ON} which results in an increase of the inductor current and consequentially of the feedback voltage.

- it does not require loop compensation network making the design easier,
- it has a faster transient response because the error amplifier is no more used.

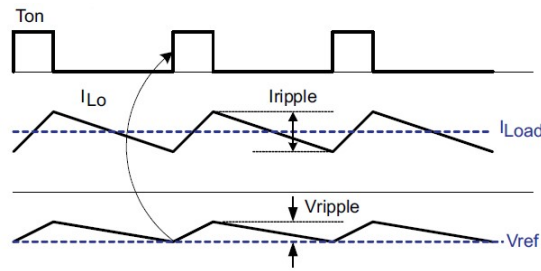


Figure 2.2: Mode of operation of a COT converter.

However, it also has as a downside a switching frequency variation with respect to the input voltage and load conditions. Thus, an adaptive approach called Adaptive Constant-On-Time (ACOT) is used to improve this control technique. The analyzed device embed this type of control method, which is able to dynamically adjust the on-time duration based on the input voltage and output voltage.

A comparison between several implementation of the three method mentioned above is represent in Figures 2.3, 2.4, 2.5 respectively.

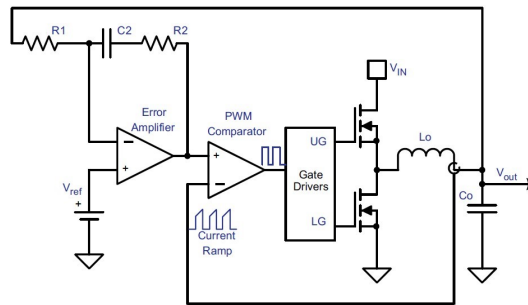


Figure 2.3: Current mode control [12].

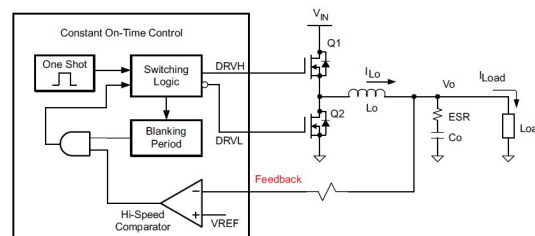


Figure 2.4: Constant-On-Time Control [12].

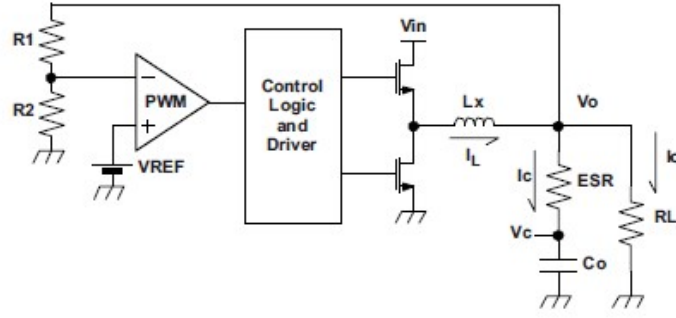


Figure 2.5: Adaptive Constant-On-Time [12].

The device used has a switching frequency of 1MHz. The input voltage range from 2.8 V to 5.5 V, instead the output voltage varies between 0.6 V to 3.9 V, the maximum output current is equal to 6 A.

2.1.1 EUT configuration

According to the regulations, the tests which allows to verify the compliance with the standard limits indicate that:

- EUT shall be installed, arranged and operated in a manner consistent with typical applications.
- EUT with more than one rated voltage shall be tested at the rated voltage which causes maximum disturbance.
- EUT shall be operated under conditions of use intended by the manufacturer which cause the maximum disturbance at the measurement frequency.

Initial testing shall identify the frequency that has the highest disturbance relative to the limit. To cope this purpose, the conditions in which the harmonic content gives the greatest contribution have been analyzed.

Using Fourier analysis, a periodic signal $S(t)$ can be represented by an infinite sum of sinusoidal components:

$$S(t) = c_0 + \sum_{n=1}^{\infty} 2|c_n| \cos(n\omega_s t + \angle c_n) \quad (2.1)$$

where n is the harmonics' order and the factor of two take into account a one-sided spectrum of positive frequencies. The coefficients c_n are defined as:

$$c_n = \frac{1}{T_s} \int_{t_0}^{t_0+T_s} S(t) e^{-jn\omega_s t} dt \quad (2.2)$$

For the trapezoidal input current of a buck converter with duty cycle d the Fourier coefficients are given by the following equation:

$$c_n(d, n) = I_{out} d \left| \frac{\sin(n\pi d)}{n\pi d} \right| \left| \frac{\sin(n\pi d_r)}{n\pi d_r} \right| \quad (2.3)$$

where a second term set by finite rise and fall times, t_R and t_F , defined the duty factor d_r . As can be seen in Figure 2.6 t_1 is the pulse width, t_S is the switching period, d is given by t_1/t_S , while t_R is the rise time, t_F is the fall time and d_r is given by t_R/t_S or t_F/t_S .

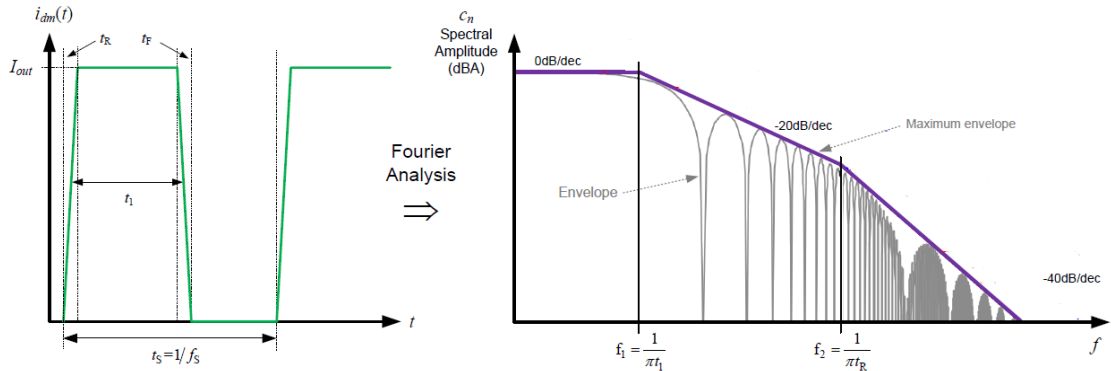


Figure 2.6: Buck converter input current waveform and spectral envelope with breakpoints determined by duty cycle rise and fall times.

Computing the Fourier coefficients, the maximum one is obtained when the output current reaches its maximum value and the duty cycle is approximately 50%, as can be seen in Figure 2.7. Hence in order to provide the maximum disturbance, the EUT used is configured with an input voltage of 5.5V and an output voltage of 2.75V, while the rated output current is 6 A. In order to obtain a compliant value even in the worst condition tested. So that with a smaller value of input voltage and output current or with a different value of duty cycle the requirements are still satisfied.

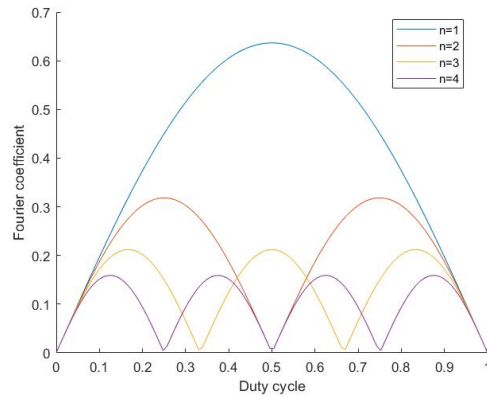


Figure 2.7: Fourier coefficient of the input current of buck converter.

2.2 LISN configuration

The connection of the LISN between the input supply and the equipment under test (EUT) provides a well defined impedance and ensures reproducibility of the measurements. Subsequently the conducted emissions are calculated through the measurement of the voltage at the LISN in units of decibel microvolts ($dB\mu V$).

The values are similar for a LISN conforming to CISPR 16-1-1 [13]. or to CISPR 25, except the LISN inductance values which are respectively $50\ \mu H$ and $5\ \mu H$.

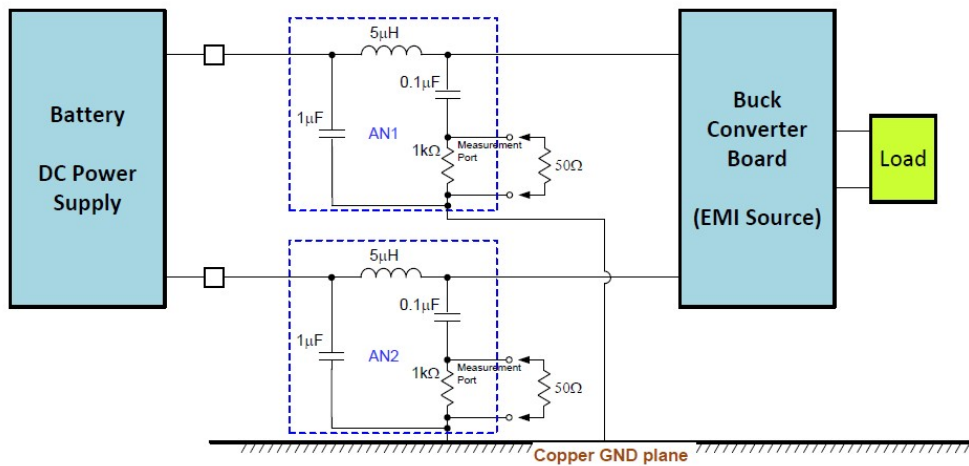


Figure 2.8: Equivalent Circuit of a Conducted Emission Test in CISPR 25 [14].

According to CISPR 16-2-1 [1], the measurement to be performed are:

- Asymmetric voltage or CM voltage, that is the voltage appearing between the electrical mid-point of the individual terminals or leads in a two or multi wire circuit and reference ground. Considering V_a as the vector voltage between one of the mains terminals and reference ground, and V_b the vector voltage between the other mains terminal and reference ground, the asymmetric voltage is half the vector sum of V_a and V_b : $(V_a+V_b)/2$,
- symmetric voltage or DM voltage, that is the voltage appearing between any pair of wires not comprising the wire at ground potential in a two or multi wire circuit. It is computed as the vector difference (V_a-V_b) ,
- unsymmetric mode voltage, that is the voltage appearing between an individual terminal or lead in a two or multi wire circuit and reference ground, and it denotes the amplitude of the vector voltage V_a or V_b .

In the case under analysis, the parasitics capacitance due to the long cabling and case are disregarded, so the analysis is focused on DM voltage.

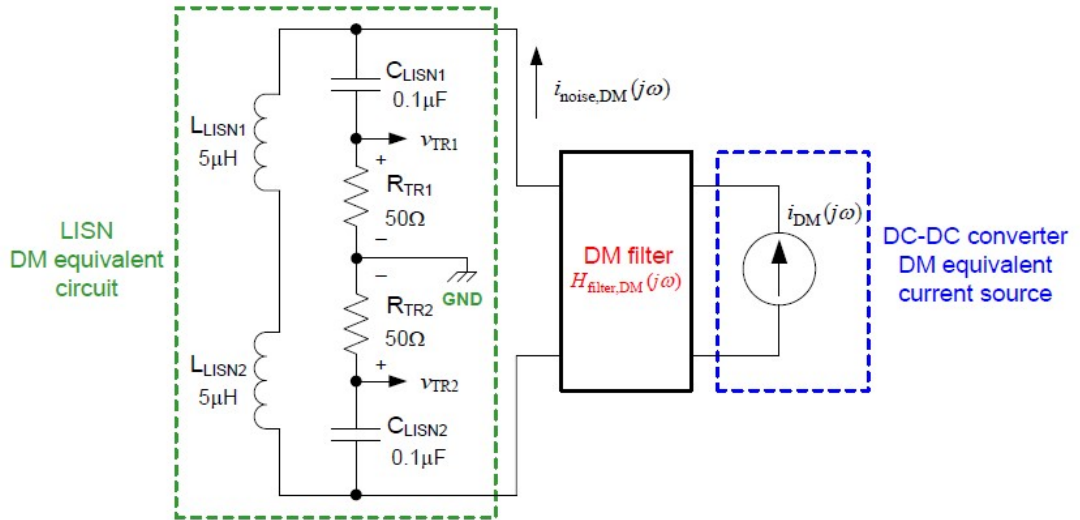


Figure 2.9: Circuit model for determining DM conducted emissions.

Figure 2.9 shows the DM equivalent circuit of the LISN and an equivalent current source denoted as i_{DM} that replaces the converter. This current source is defined by the spectral composition of the converter input current waveform, which in the case of a buck converter is a trapezoidal input current waveform.

Therefore, the final LISN used for simulation of the conducted disturbance is the following:

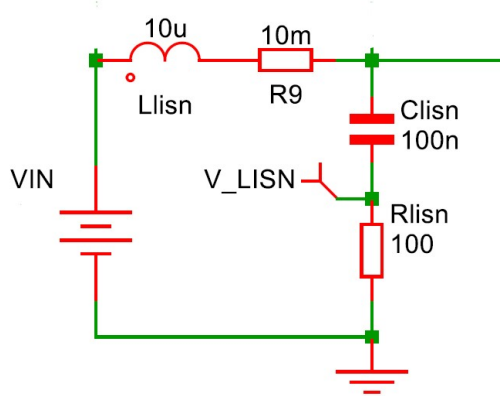


Figure 2.10: Final model of DM LISN.

The LISN transfer function from the DM noise current to the LISN resistor voltage when it is connected to the test receiver (TR) is:

$$G_{LISN}(s) = \frac{v_{R_{lisen}}(s)}{i_{noise,DM}(s)} = R_{LISN} \frac{s^2 L_{LISN} C_{LISN}}{s^2 L_{LISN} C_{LISN} + s C_{LISN} R_{LISN} + 1} \quad (2.4)$$

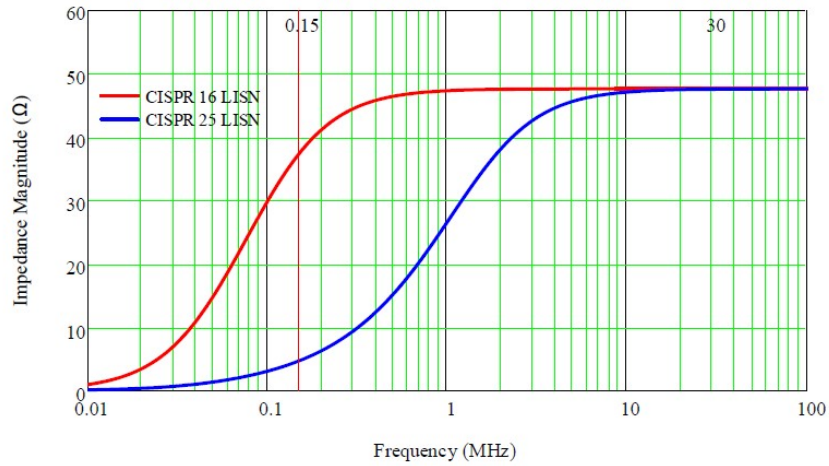


Figure 2.11: LISN transfer function from noise current to measured voltage.

2.3 Test receiver configuration

Lately a time-domain mathematical model of the EMI receiver has been developed. The output of the mixer is the input signal shifted by the output frequency of the local oscillator as can be seen in Figure 2.12 Changing the frequency of the local oscillator the part of the input spectrum centered at the intermediate frequency (IF) is selected.

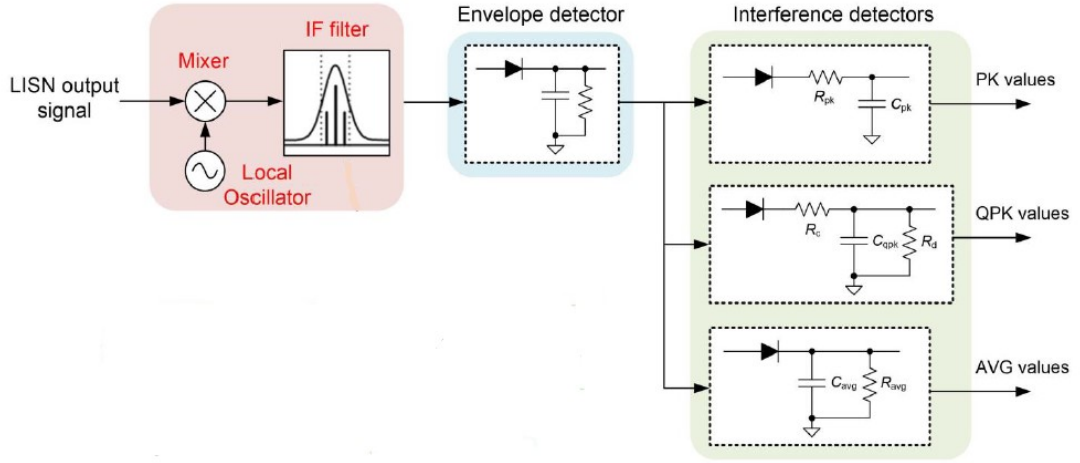


Figure 2.12: Model of the test receivers [15].

The amplitude gain of the equivalent IF filter based on near-Gaussian filter theory can be expressed as:

$$|G_{IF}(f, f_{IF})| = e^{-\left[\frac{(f-f_{IF})\sqrt{\ln 2}}{f_{RBW}/2}\right]^2} = \begin{cases} 0 \text{ dB at } f = f_{IF} \\ -6 \text{ dB at } f = f_{IF} \pm f_{RBW}/2 \end{cases} \quad (2.5)$$

Where f_{IF} is the center frequency of the equivalent IF filter, according to CISPR 16-1-1 the resolution bandwidth (RBW) of the IF filter is 200 Hz from 9 kHz to 150 kHz and 9 kHz from 150 kHz to 30 MHz.

Just after the envelope detector, there are sundry types of detector used for EMI measurement: peak (PK), quasi-peak (QPK) and average (AVG). The equation to compute the detector output voltage are:

$$V_{peak} = \max(V_i) \quad (2.6)$$

$$\frac{\sum_{i=1}^Q \left(V_i - V_{quasi-peak} \right)}{R_c} = \frac{V_{quasi-peak} N}{R_d} \quad (2.7)$$

$$V_{avg} = \frac{\sum_{i=1}^N V_i}{N} \quad (2.8)$$

where N are points uniformly sampled in one period, the results of V_{peak} and V_{avg} represent the maximum and averaged values of the points that have been sampled. Instead, the $V_{quasi,peak}$ computation is made possible thanks to charge balance on the detector capacitor [15].

Generally, $V_{peak} \geq V_{quasi-peak} \geq V_{avg}$, while in the case of a constant pulsewidth waveform, when the output voltage of the envelope detector has only a DC component, $V_{peak} = V_{quasi-peak} = V_{avg}$.

A constant pulsewidth modulation waveform with a fixed frequency $f_s = 1/T$ and duty cycle D is considered. The switching frequency is usually much higher than the resolution bandwidth in the standard for conductive EMI (200 Hz RBW for band A and 9 kHz RBW for band B). If $k = 2RBW/f_s \leq 1$, only a single frequency component is within the two RBW effective bandwidth of the IF filter as depicted in Figure 2.13, and the output time-domain signal of the IF filter has only one frequency component.

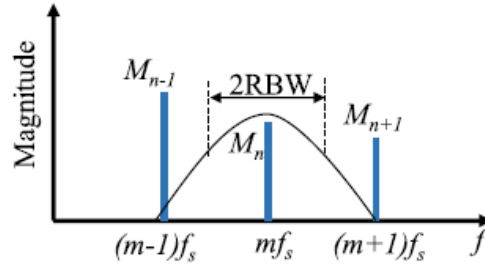


Figure 2.13: IF filter with smaller effective bandwidth than harmonic frequency interval [16].

Since this frequency component has a constant magnitude the envelope of the waveform is dc. For a dc envelope signal the peak, quasi-peak, and average values are equal, therefore the three measurements turn out to be equal. In this context, they result to be equal also to FFT, because with FFT the spectrum of the magnitudes of all the individual frequency components is computed. Therefore $V_{peak} = V_{quasi-peak} = V_{avg} = V_{FFT}$.

According to regulations, the decision tree in Figure 2.14 must be observed to comply with the standards.

The measured peak value must be compared with the average limit value and if it is lower the EUT pass the test. Otherwise the comparison is done with the quasi-peak limit: if the peak value is lower than the quasi-peak limit the condition to be checked is that the measured average value is less than the average limit. And if this condition is verified the test is passed otherwise it fails. Finally if the initial comparison between the peak value and the quasi-peak limit leads to a higher value of the measured peak, the quasi-peak measurement has to be lower to the quasi-peak limit to proceed the test otherwise the EUT is not conform. Now if the quasi peak value is lower than the average limit the test is passed otherwise the initial condition on the average value need to be checked.

Since the values of the peak, quasi-peak and average in the case study are equal, the FFT of the LISN measured voltage is performed and it is compared with the standard limit of the average voltage.

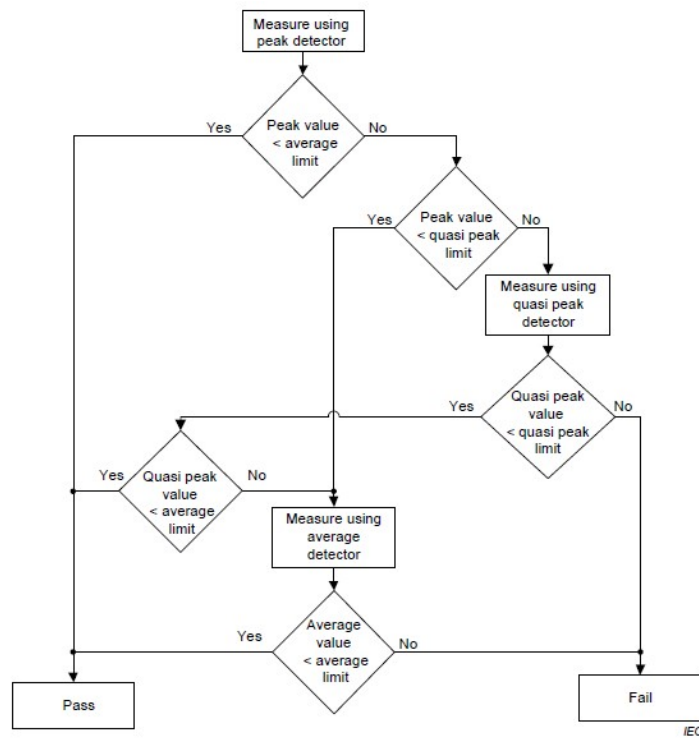


Figure 2.14: Decision tree for using different detectors with quasi peak and average limits [1].

In conclusion, a reliable environment was obtained to carry out the simulations. The device is configured according to the required specification during the testing process and the employed measuring instruments and their characteristics have been defined.

Chapter 3

Design of input filter

3.1 Specification analysis

The availment of switching converter almost always requires the use of an input filter that attenuate the harmonics present in the input current, ensuring compatibility with standard EMC regulations. The main purposes of the introduced input filters are:

- ensuring an almost dc input current removing the ac harmonic content,
- preventing both DM and CM EMI generated by the switching source from reaching the input power lines,
- protecting the converter and the load from disturbance in entrance as surges, dips and bursts.

Therefore the goals for filter design should be to:

- meet the international attenuation requirements of conducted emissions,
- limit the physical size and stored energy of the components,
- minimize the total filter cost.

The design of the EMI filter is an iterative process, starting from measurement, simulation or computation of the DM and CM noise, comparing it to the emission limit and obtaining the required attenuation, the filter topology and the components can be selected. Afterwards an evaluation phase is done, verifying that the requisites have been met, otherwise the test it not passed and a reassessment of the components selected must be done.

This section discusses the analysis for the design of a filter for the differential mode.

Therefore the necessary attenuation must be defined first. It is computed as explained in [17]:

$$A_{dm}[dB] = A_{dm-nofilter}[dB\mu V] - A_{std}[dB\mu V] + m[dB\mu V] \quad (3.1)$$

where $A_{dm-nofilter}$ is the amplitude of the maximum unfiltered conducted noise voltage, A_{std} is the value of the standard limit and m is a safety margin, typical of 2-6 dB μV . The value of the required attenuation depends on the amplitude of the first harmonic (usually on the amplitude of the fundamental, if instead the switching frequency is lower than 150kHz, that is the bottom limit for conducted emission, it is determined by the second or third harmonic). Since the Fourier series for the DM input current of a buck converter is given by:

$$i_{in,buck}(t) = I_{out}D + \sum_{n=1}^{\infty} \frac{2I_{out}}{n\pi} \sin(n\pi D) \cos(n\omega t) \quad (3.2)$$

the required attenuation is obtained by computing the first harmonic amplitude from the Fourier series of the input current waveform and multiplying it by the impedance defined by the converter input capacitance:

$$A_{dm}[dB] = 20 \log \left(\frac{I_{out}}{\pi f_s C_{in}} \cdot \frac{\sin(\pi D)}{\pi} \cdot \frac{1}{\mu V} \right) - A_{std}[dB\mu V] + m[dB\mu V] \quad (3.3)$$

For the case in analysis the output current is equal to 6A, f_{sw} is 1MHz, the duty cycle is 50% and C_{in} value is 4.7 μF with a parasitic resistance of 5m Ω . The CISPR limit used for conducted emission is 46dB μV and a safety margin of 2dB μV was taken. Therefore the attenuation obtained is:

$$A_{dm}[dB] = 102[dB\mu V] - 46[dB\mu V] + 2[dB\mu V] \quad (3.4)$$

A similar result is obtained with the simulation:

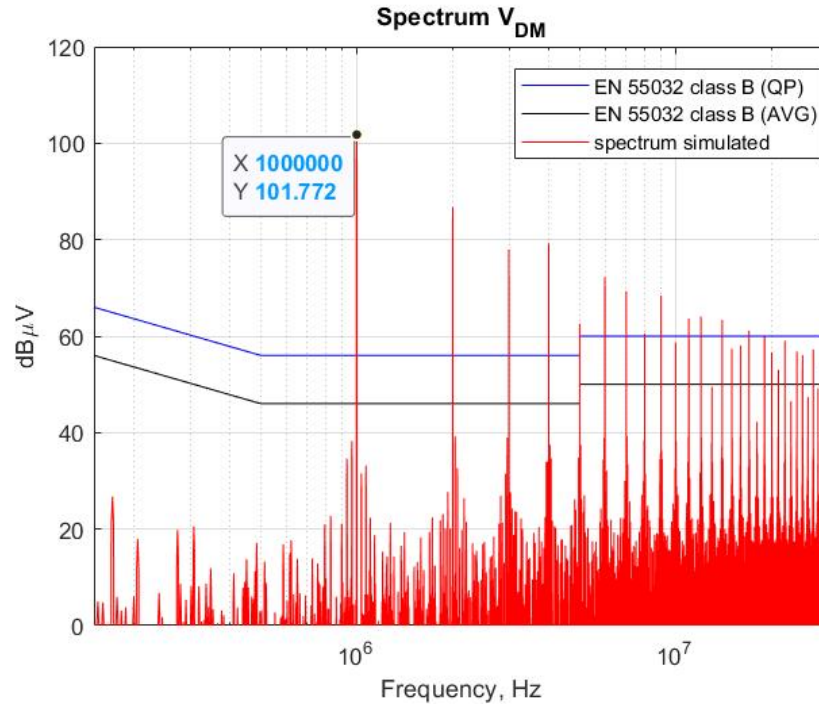


Figure 3.1: Simulated spectrum of DM voltage.

Thus the final attenuation used for the design of the filter is 58dB.

3.2 Impact on stability

Now the interaction between EMI filter and dc-dc converter is examined, deepening its impact on overall system stability.

A switching regulator that responds properly to any input voltage variation, maintains the dc output voltage constant and unperturbed. Therefore for a given load, the output power is constant independently of input voltage, as the average input power (assuming no losses). If the input voltage increases, the duty factor is reduced to keep constant output voltage, causing the average input current to be consequently decreased. The input current decreases as a result of an increase of the input voltage, as a negative dynamic resistance:

$$\frac{\partial v}{\partial i} = \frac{\partial}{\partial i} \left(\frac{P}{i} \right) = -\frac{P}{i^2} = -\frac{v^2}{P} = R_{in} \quad (3.5)$$

This model is not linear since R_{in} is a function of v . However, in the proximity of a given operating point it can be considered constant as described in [18]. The input resistance can also be obtained expressing the input voltage and current as a function of the duty cycle:

$$v(D) = \frac{v_{out}}{D} \quad i(D) = i_{out}D \quad (3.6)$$

$$\partial v = -\frac{v_{out}}{D^2} \partial D \quad \partial i = i_{out} \partial D \quad (3.7)$$

$$\frac{\partial v}{\partial i} = -\frac{v_{out}}{i_{out}D^2} \rightarrow R_{in} = -\frac{R_L}{D^2} \quad (3.8)$$

For the stability study, a general case of two individually stable subsystems cascaded can be considered:

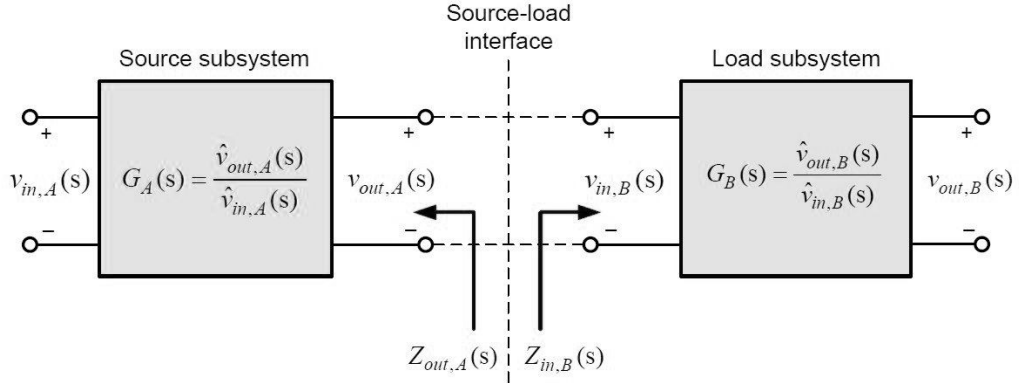


Figure 3.2: Cascaded connection of two stable and independent subsystem [19].

Indicating with $Z_{out,A}(s)$ and $Z_{in,B}(s)$ the output impedance of the source subsystem and the input impedance of the load subsystem respectively, and with $G_A(s)$ and $G_B(s)$ the stand alone-stable small-signal transfer functions, the following expression can be obtain:

$$\frac{\hat{v}_{out,B}(s)}{\hat{v}_{in,A}(s)} = G_A(s)G_B(s) \frac{Z_{in,B}(s)}{Z_{in,B}(s) + Z_{out,A}(s)} = \frac{G_A(s)G_B(s)}{1 + T_M(s)} \quad (3.9)$$

$$T_M(s) = \frac{Z_{out,A}(s)}{Z_{in,B}(s)} \quad (3.10)$$

the interaction between the two subsystem is described by the factor $1/(1 + T_M(s))$, where $T_M(s)$ is the minor-loop gain used to evaluate the state of stability of the interconnected system.

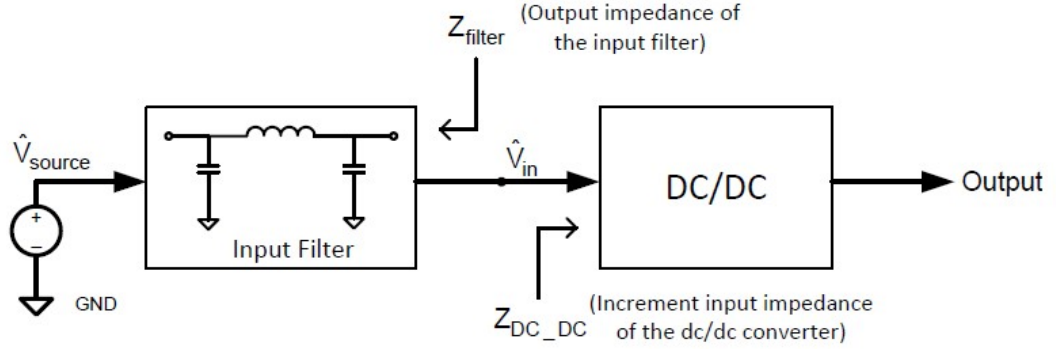


Figure 3.3: Small voltage change subdivided at input of DC/DC Converter with input filter [20].

Applying it to the dc-dc converter with its input filter, the small-signal transfer function of the interconnected system is:

$$\frac{\hat{V}_{in}(s)}{\hat{V}_{source}(s)} = \frac{Z_{DC_DC}(s)}{Z_{DC_DC}(s) + Z_{filter}(s)} = \frac{1}{1 + \frac{Z_{filter}(s)}{Z_{DC_DC}(s)}} \quad (3.11)$$

with the minor loop gain equal to:

$$T_M(s) = \frac{Z_{filter}(s)}{Z_{DC_DC}(s)} \quad (3.12)$$

now using the Nyquist criterion the condition of oscillations are:

$$\left| \frac{Z_{filter}(s)}{Z_{DC_DC}(s)} \right| = 1 \quad \angle \frac{Z_{filter}(s)}{Z_{DC_DC}(s)} = -180^\circ \quad (3.13)$$

Therefore a sufficient condition for stability is that:

$$\begin{aligned} |T_M(s)| &= \left| \frac{Z_{filter}(s)}{Z_{DC_DC}(s)} \right| \ll 1 \\ |Z_{filter}(j\omega)| &\ll |Z_{DC_DC}(j\omega)| \quad , \forall \omega \end{aligned} \quad (3.14)$$

3.3 Impact on performance

The input filter affects the dynamics of the converter, therefore an evaluation on the way in which it changes must be performed. For this purpose the Middlebrook's extra element theorem is used to show the variation of the transfer function with the addition of an impedance to the system.

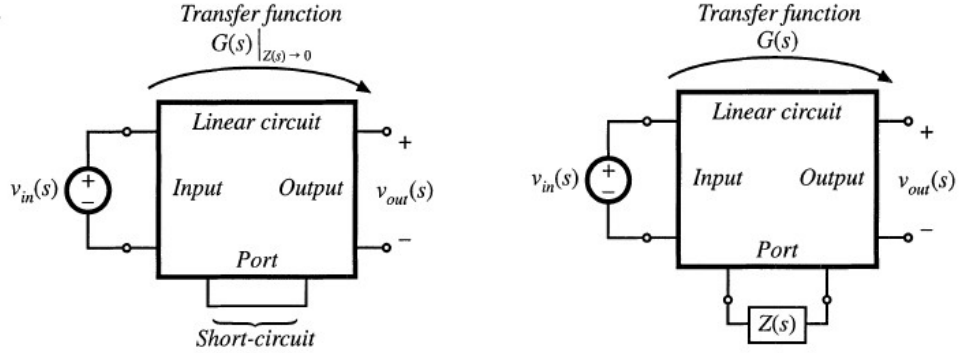


Figure 3.4: Initial conditions and addition of element having impedance $Z(s)$.

Considering a linear circuit and assuming that the transfer function from $v_{in}(s)$ to $v_{out}(s)$ is known, and is given by:

$$\frac{v_{out}(s)}{v_{in}(s)} = \left(G(s) \Big|_{Z_s \rightarrow 0} \right) \quad (3.15)$$

when the short circuit is replaced by the impedance $Z(s)$ the transfer function becomes:

$$\frac{v_{out}(s)}{v_{in}(s)} = \left(G(s) \Big|_{Z(s) \rightarrow 0} \right) \left(\frac{1 + \frac{Z(s)}{Z_N(s)}}{1 + \frac{Z(s)}{Z_D(s)}} \right) \quad (3.16)$$

In the case of the converter represented in Figure 3.5 the extra element is the output impedance $Z_o(s)$ of the added input filter while the control-to-output transfer function is:

$$G_{vd}(s) = \frac{\hat{v}(s)}{\hat{d}(s)} \Big|_{\hat{v}_g(s)=0} \quad (3.17)$$

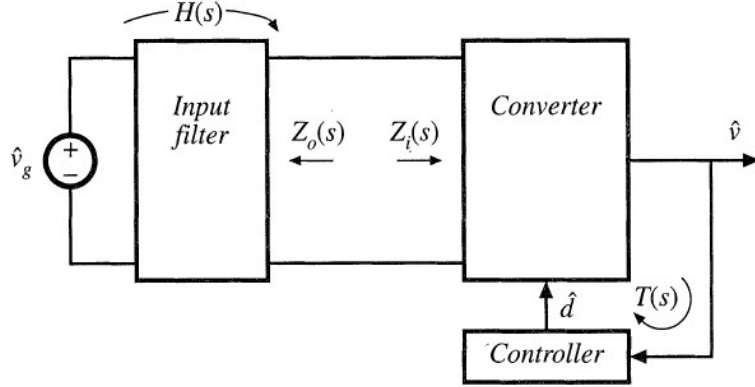


Figure 3.5: Switching voltage regulator with its input filter.

Thus the control-to-output transfer function with the insertion of the filter becomes:

$$G_{vd}(s) = \left(G_{vd}(s) \Big|_{Z_0 \rightarrow 0} \right) \left(\frac{1 + \frac{Z_0(s)}{Z_N(s)}}{1 + \frac{Z_0(s)}{Z_D(s)}} \right) \quad (3.18)$$

where $G_{vd}(s) \Big|_{Z_0 \rightarrow 0}$ is the control-to-output transfer without the presence of the input filter.

- The value of $Z_D(s)$ (Figure 3.6) is the Thevenin equivalent impedance seen looking into the port by setting the input source $v_{in}(s)$ to zero, and then measuring the impedance among the port terminals, that in the case of buck converter it's equal to the converter input impedance $Z_i(s)$ under the condition that $\hat{d}(s)$ is equal to zero, this value coincides with the open-loop input impedance of the converter:

$$Z_D(s) = Z_i(s) \Big|_{\hat{d}(s)=0} \quad (3.19)$$

$$Z_{D,buck}(s) = \frac{1}{D^2} \left(sL + R \parallel \frac{1}{sC} \right) \quad (3.20)$$

$$Z_{D,buck}(s) = \frac{R}{D^2} \frac{\left(1 + \frac{sL}{R} + s^2LC \right)}{(1 + sRC)} \quad (3.21)$$

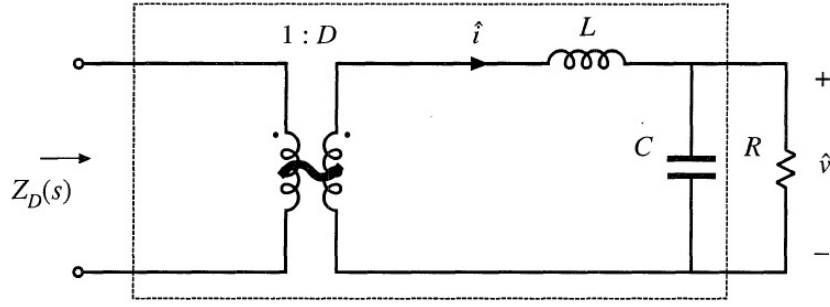


Figure 3.6: Small-signal model of buck converter for the determination of Z_D .

- The value of $Z_N(s)$ (Figure 3.7) is found under the conditions that the output $v_{out}(s)$ is nulled. The value of $v_{out}(s)$ can be obtained from a linear combination of $v_{in}(s)$ and $i(s)$ therefore exist always a possible choice of $i(s)$ that causes the output to be nulled.

In the case of the buck it is equal to the converter input impedance $Z_i(s)$ under the condition that the feedback controller operates ideally varying $\hat{d}(s)$ in order to maintain $\hat{v}(s)$ equal to zero, and it coincides with the impedance that would be measured at the converter input terminals, if an ideal feedback loop perfectly control the converter output voltage. It is computed injecting a test current at the converter input port, due to the fact that the voltage $\hat{v}(s)$ is zero, the currents in the capacitor and in the load is zero, thus the current in the inductor and in the transformer winding is also null and it follows that the voltage across the inductor is zero. As a result the voltage applied to the secondary of the transformer is equal to the source voltage $-V_g \hat{d}(s)$, and the current $\hat{i}_{test}(s)$ is equal to the current source $I \hat{d}(s)$:

$$Z_N(s) = Z_i(s) \Big|_{\hat{v}(s) \rightarrow 0} \quad (3.22)$$

$$Z_{N,buck}(s) = \frac{\left(-\frac{V_g \hat{d}(s)}{D}\right)}{I \hat{d}(s)} \quad (3.23)$$

$$Z_{N,buck}(s) = -\frac{R}{D^2} \quad (3.24)$$

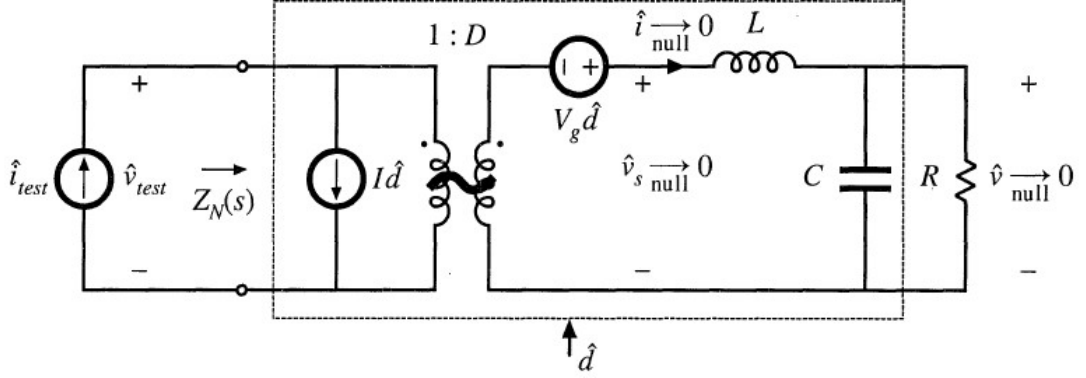


Figure 3.7: Small-signal model of buck converter for the determination of Z_N .

The complete demonstration to find the value of Z_N , Z_d is described in [21]. In general the inequalities that guarantee that the transfer function is not significantly modified occurs when:

$$\|Z(j\omega)\| \ll \|Z_N(j\omega)\| \quad (3.25)$$

$$\|Z(j\omega)\| \ll \|Z_D(j\omega)\| \quad (3.26)$$

In this specific case to not change substantially the control-to-output transfer function the correction factor $\left(\frac{1 + \frac{Z_o(s)}{Z_N(s)}}{1 + \frac{Z_o(s)}{Z_D(s)}}\right)$ has to be approximately equal to unity, that means:

$$\|Z_o\| \ll \|Z_N\| \quad (3.27)$$

$$\|Z_o\| \ll \|Z_D\| \quad (3.28)$$

if these constrains are satisfied the magnitude of the correction factor is almost equal to 1. Therefore these equations represent a limit on the maximum possible value of the output impedance of the inserted filter, setting a criterion for the design of the filter.

A similar analysis could be done for the converter output impedance, deriving the expression that guarantee that the output impedance is not substantially affected by the insertion of the input filter:

$$\|Z_o\| \ll \|Z_e\| \quad (3.29)$$

where $Z_e(s)$ is the converter input impedance under the condition that the output of the converter is shorted:

$$Z_e(s) = Z_i(s) \Big|_{\hat{v}_e=0} \quad (3.30)$$

$$Z_{e,buck}(s) = \frac{sL}{D^2} \quad (3.31)$$

The coexistence of an EMI filter and a switched-mode converter determines a system that is subjected to instability and worsening of performance. The overlap between the input impedance of the converter and resonant behavior of the output impedance of the filter may occur if some precautions are not adopted, as for example the damping, that preserve the dynamic performance of the converter, where the significant elements of the dynamic profile are:

- the control-to-output transfer function that gives a contribution on the output-voltage loop gain,
- the open loop output impedance that determines the the load interactions.

Chapter 4

Passive filter

The most employed solutions to decrease the interference signal at switching frequency and its harmonic content which go back to the power supply is to implement and add to the system a passive design. Occupying from 25% to 50% of the total converter dimension, a compact and efficient EMI filter implementation is one of the most critical challenges in high-density dc-dc converter designs.

Numerous different DM passive filter topology are theoretically available for EMI filtering [22], instead practically only a few are commonly used, for reasons related to cost and complexity.

The filter topologies studied in this chapter are the LC and π -type that are able to attenuate the high frequency noise from the power supply and suppress the switching noise to return to it. Knowing the magnitude of the effective noise source and filter's load impedance the filter parameter calculations can be addressed.

4.1 LC filter

The first passive solution implemented is with the use of an undamped LC filter. An overview of LC filter is present in [22]. It is a second order filter that ideally provides 40dB per decade of attenuation after the cutoff frequency f_c , it has no gain before f_c , and it presents a gain peak at the resonant frequency which subsequently needs to be reduced in order to not interfere with the stability of the system.

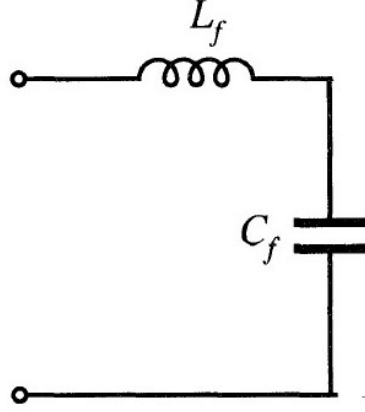


Figure 4.1: LC circuit.

The attenuation of the current from the input to the output of the filter can be expressed in the following way:

$$\frac{I_{out,filter}(s)}{I_{in,filter}(s)} = \frac{1}{1 + s^2 L_f C_f} \quad (4.1)$$

instead the corner frequency is equal to:

$$f_c = \frac{1}{2\pi\sqrt{L_f C_f}} \quad (4.2)$$

therefore for having the wanted attenuation at the switching frequency, that is the one that gives the higher contribution that must be reduced, the corner frequency should be chosen in order to have:

$$A_{dm} = \left(\frac{f_{sw}}{f_c}\right)^2 \quad \rightarrow \quad A_{dm}[dB] = 40 \log\left(\frac{f_{sw}}{f_c}\right) \quad (4.3)$$

$$f_c = \frac{f_{sw}}{10^{A_{dm}[dB]/40}} \quad (4.4)$$

Subsequently a more in-depth analysis is performed computing the current attenuation from the input of the converter to the LISN, which is the measure that is carried out to verify that the system is up to standard. Considering the impact of the LISN on the value of the attenuation, where C_{in} is the input capacitance of the converter with its ESR and $Z_{o,LISN}$ is the output impedance of the LISN:

$$\frac{I_{in,buck}(s)}{I_{out,R_{LISN}}(s)} = \frac{\frac{1}{sC_f} // \left(\frac{1}{sC_{in}} + R_{C_{in}}\right)}{\frac{1}{sC_f} // \left(\frac{1}{sC_{in}} + R_{C_{in}}\right) + sL_f + Z_{o,LISN}} \frac{L_{LISN}}{L_{LISN} + C_{LISN} + R_{LISN}} \quad (4.5)$$

By choosing different possible combinations of values for L_f and consequently for C_f that guarantee the same attenuation without initially considering the impedance of the LISN, it leads to a subsequent variation of the attenuation level when in the analysis the filter is closed with the output impedance of the LISN. Therefore the values of L_f and C_f are recomputed, finding the different couples that even with the LISN impedance generate the final same attenuation at the switching frequency.

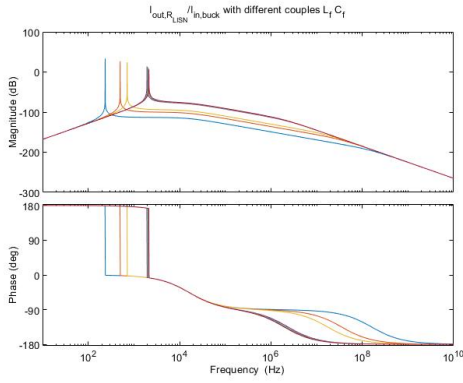


Figure 4.2: Attenuation for different couples of L_f C_f not considering LISN interaction.

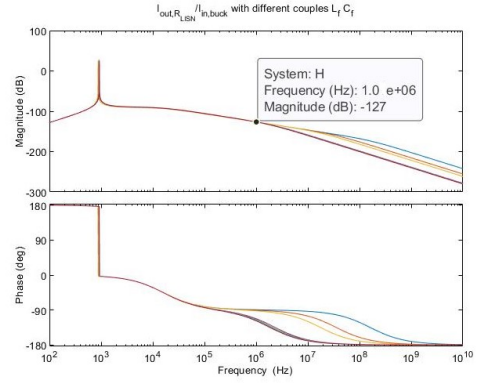


Figure 4.3: Attenuation for different couples of L_f C_f considering LISN interaction in order to have the same final attenuation at the switching frequency.

For the analysis of the stability of the system in which the filter is inserted and for the assessment of the impact of the filter on overall performance the output impedance of the LC filter is computed:

$$Z_{out,LC} = L_f // C_f // C_{in} \quad (4.6)$$

The basic principle to avoid the stability issue is to obtain an output impedance of the filter lower than the input impedance of the converter, and to minimize the impact of correction factor introduced by the input filter to not modify the control-to-output transfer function, the output impedance of the filter should be lower than Z_N and Z_D . Therefore $Z_{out,LC}$ is compared with the quantity Z_{in} , Z_D , Z_N , Z_e obtained as explained in chapter 3, in the condition in which the converter produces the minimum value of these quantities in order to ensure stability and reduce the correction factor even in the worst case.

In the following Figures is possible to see that the output impedance of the

filter approaches infinity at the resonance frequency, and the limits are exceeded. Thus stability is not ensured and the control-to-output transfer function is modified.

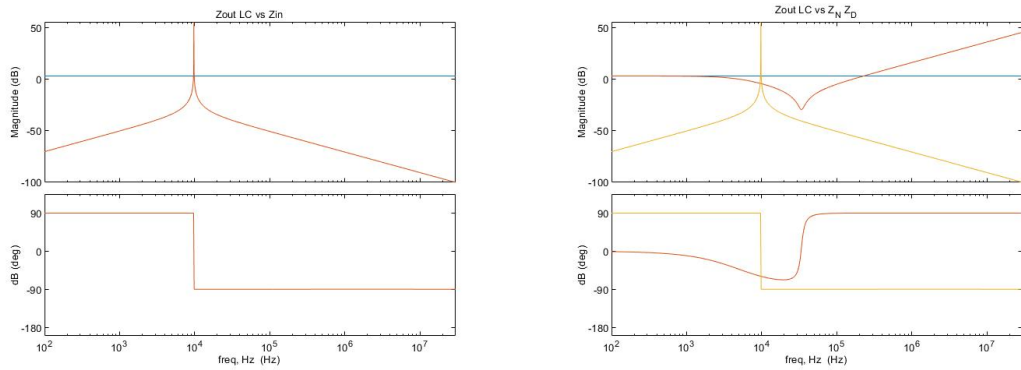


Figure 4.4: $Z_{out,LC}$ compared with $Z_{in,buck}$. **Figure 4.5:** $Z_{out,LC}$ compared with Z_N and Z_D .

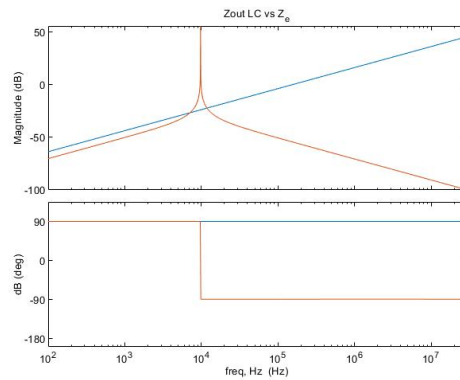


Figure 4.6: $Z_{out,LC}$ compared with Z_e .

Therefore to control the impedance peaking, damping is necessary. In order to reduce the peak of the output impedance at the resonant frequency and do not go beyond the limit.

4.1.1 Damping

In the worst case we can assume that the output impedance of the energy source is a very low impedance and so the LC EMI filter will experience a parallel resonance that can be very sharp, therefore damping must be provided to make sure that it does not cause undesired effects. The problem is that when a parallel resonant tank is excited at that resonant frequency there is an enormous amount of circulating current, even a small excitation at that frequency can excite an important value of that current in the resonant tank and the loop containing this parallel resonant tank include the input branch, so the large circulating current circulate through the source and it is an unwanted EMI.

Damping must also be provided to overcome the negative equivalent input resistance of the converter. As seen previously, if the converter was realized with a good design, there is a constant power load: the power converter will draw the same amount of power regardless variation in the input voltage, and linearizing this load at a given operating point the input resistance can be expressed as:

$$R_{in,conv} = -\frac{P}{I_{in}^2}.$$

Therefore to damp the filter a resistor R_f can be added in parallel to the capacitor C_f .

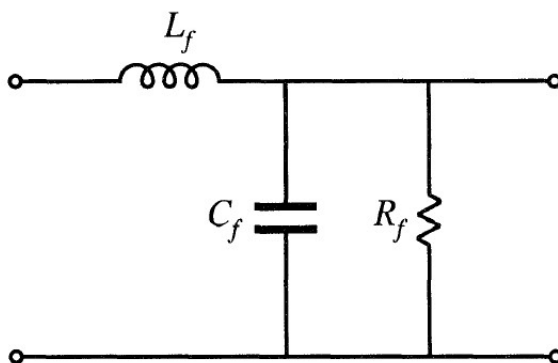


Figure 4.7: Damping with R_f in parallel with C_f .

This filter is then closed with the negative resistance of the converter and in order to prevent the instability the figure of merit must be figured out.

$$Q = R_{eq} \sqrt{\frac{C_f}{L_f}} \quad (4.7)$$

where R_{eq} is equal to:

$$R_{eq} = \frac{R_f \cdot R_{in,conv}}{R_f + R_{in,conv}} \quad (4.8)$$

the numerator of the quality factor is always negative, so the only way for the quality factor to be positive is that also the denominator is negative. Thus a value of R_f less than the magnitude of $R_{in,conv}$ is needed.

In addition, to guarantee an acceptable damping, the value of Q have to be equal to 1.

Both of this requirement lead to the same conclusion, a small resistance R_f is required. But this solution generates an issue because of the power dissipation in R_f . The dc input voltage V_g is applied across resistor R_f , and the smaller is the resistor the higher is the power consumption therefore it dissipates a power equal to V_g^2/R_f that implies a power loss greater than the load power. In conclusion it is not a feasible solution.

To solve the problem of the power loss, R_f could be placed in parallel to L_f (Figure 4.8). Since the dc voltage across inductor L_f is null, there is now no dc power loss in resistor R_f . The problem now is that the transfer function contains a high-frequency zero: the addition of R_f degrades the slope of the high frequency asymptote, from -40 dB/dec to -20 dB/dec, therefore L_f must be large in order to obtain the same attenuation as a simple LC filter.

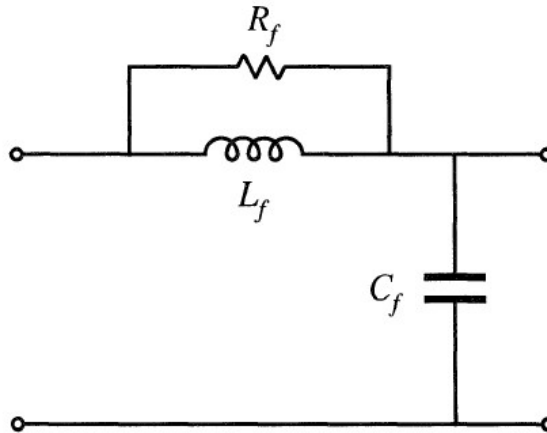


Figure 4.8: Damping with R_f in parallel with L_f .

Problems also occur if the damping resistor is placed in series with L_f because the efficiency is heavily degraded, since all the dc input current pass through it. Instead if the damping resistor is placed in series with C_f the attenuation of the filter is degraded.

One practical solution is to put the R_f in parallel to C_f and add in series to the resistor a blocking capacitor C_b in order that no dc current can flow through R_f and the dc power loss is nulled.

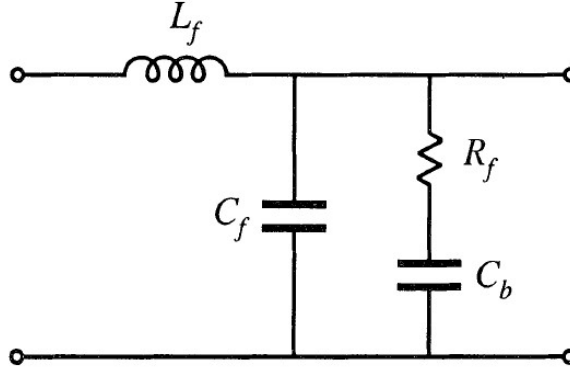


Figure 4.9: Damping with the parallel of R_f in series with C_b .

So the behavior of the capacitor is needed at low frequency and the behavior of the resistor is needed at high frequency, therefore the value of the capacitor C_b is chosen in order to be very large such that at the filter resonant frequency the impedance of this new branch added to the filter is dominated by the resistor. Commonly used value for these elements are [24]:

$$R_f = \sqrt{\frac{L_f}{C_f}} \quad (4.9)$$

$$C_b > 5C_f \quad (4.10)$$

so we can use an electrolytic capacitor that has a very large capacitance but also a reasonable sized ESR and all the damping leg can be created with a single component.

An alternative to the choice of the values of R_f and C_b finding the optimal damping is implemented in the following way. First the new output impedance of the filter has to be recomputed considering $C_b = nC_f$:

$$Z_{out}(s) = sL_f \frac{1 + sR_f C_b}{1 + sC_b R_d + s^2 L_f (C_b + C_f) + s^3 (L_f C_b C_f R_f)} \quad (4.11)$$

$$Z_{out}(s) = sL_f \frac{1 + sR_f n C_f}{1 + sn C_f R_d + s^2 L_f C_f (1 + n) + s^3 (L_f n C_f^2 R_f)} \quad (4.12)$$

Now substituting the Middlebrock's definitions: $R_0 = \frac{L_f}{C_f}$, $Q = \frac{R_f}{R_0}$, $\omega_0 = \frac{1}{\sqrt{L_f C_f}}$ and considering $x = \frac{\omega}{\omega_0}$, the final expression obtained for the output impedance is:

$$|Z_{out}(\omega)| = R_0 \frac{x\sqrt{1+n^2Q^2x^2}}{\sqrt{[1-(1+n)x^2]^2 + [xnQ(1-x^2)]^2}} \quad (4.13)$$

To reduce the peaking of the function we have to find the minimum of the output impedance with respect to the Q factor, therefore the sensitivity of Z_{out} respect to Q is computed, working on Z_{out}^2 to get rid of the square root:

$$\frac{d}{dQ}(Z_{out}(Q)^2) = \frac{d}{dQ} \left(R_0^2 \frac{x^2(1+n^2Q^2x^2)^2}{[1-(1+n)x^2]^2 + [xnQ(1-x^2)]^2} \right) \quad (4.14)$$

subsequently the derivative is imposed to be equal to zero:

$$\frac{d}{dQ}(Z_{out}(Q)^2) = \frac{2Qn^3x^6(nx^2+2x^2-2)}{D(Q)} = 0 \quad (4.15)$$

$$\begin{cases} nx^2 + 2x^2 - 2 = 0 \\ x^2(n+2) = 2 \\ x = \sqrt{\frac{2}{2+n}} \end{cases}$$

and replacing the corresponding value $x = \frac{\omega}{\omega_0}$, the point at which Q_{opt} occur is obtained:

$$\omega_{opt} = \sqrt{\frac{2}{2+n}}\omega_0 = \sqrt{\frac{2}{(2+n)L_f C_f}} \quad (4.16)$$

Afterwards the value of Z_{out} at ω_{opt} is obtained substituting ω_{opt} in the initial expression 4.13:

$$|Z_{out}(\omega_{opt})| = \frac{\sqrt{2(2+n)}}{n} R_0 \quad (4.17)$$

and minimizing Z_{out} at ω_{opt} differentiating Z_{out}^2 with respect to x^2 also the optimum Q can be derived:

$$Q_{opt} = \sqrt{\frac{(4+3n)(2+n)}{2n^2(4+n)}} \quad (4.18)$$

Consequently after the choice of L_f and C_f and knowing the target value for $|Z_{out}|_{mm}$ that is the minimum value that the filter output impedance can assume in order to be lower than the converter input impedance, the value of n is defined as:

$$\begin{cases} R_0 = \sqrt{\frac{L_f}{C_f}} \\ \frac{|Z_{out}|_{mm}}{R_0} = \sqrt{\frac{2(2+n)}{n^2}} \end{cases}$$

$$n = \frac{R_0 \left(R_0 + \sqrt{R_0^2 + 4(|Z_{out}|_{mm})^2} \right)}{(|Z_{out}|_{mm})^2} \quad (4.19)$$

thus the actual value of Q_{opt} can be computed and the value of the damping component is obtained as $R_f = R_0 Q_{opt}$ and $C_b = n C_f$. The complete demonstration is described in [25].

Furthermore for the damping, two possible approach are possible: only decreasing the output impedance of the filter applying a resistor in parallel with the damping capacitor may lead into a very big and expensive damping capacitor for the required application, therefore another possibility is to keep the filter resonant frequency away from the crossover frequency of the converter. This second approach leaves more margin for the damping around the resonant frequency of the filter, making sure that the stability criterion are not violated. But in this case it is possible that the values of the components of the filter itself become too big.

In the following Figures the reduction of the peak is clearly visible where the same analysis on stability and variation of performance is performed considering the same filter with the addition of the optimum damping.

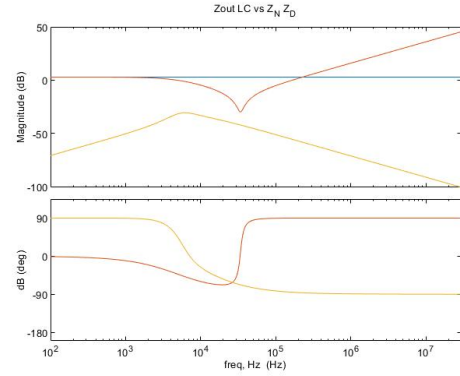
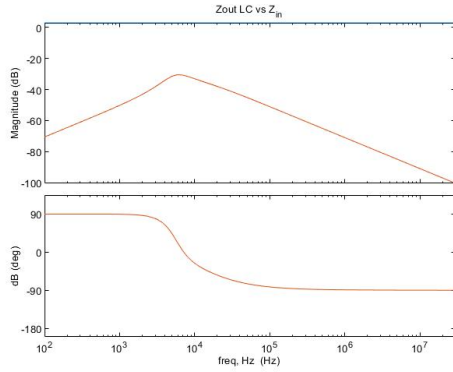


Figure 4.10: $Z_{out,LC}$ with damping compared with $Z_{in,buck}$. **Figure 4.11:** $Z_{out,LC}$ with damping compared with Z_N and Z_D .

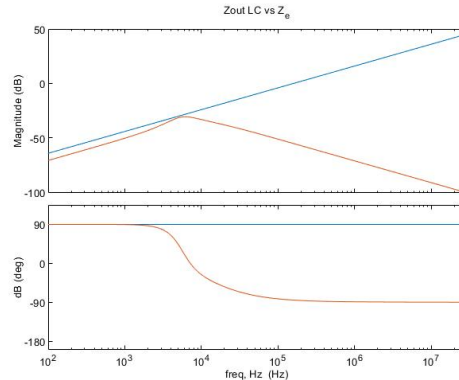


Figure 4.12: $Z_{out,LC}$ with damping compared with Z_e .

A comparison of the control-to-output transfer function of a buck converter and the input filter with and without damping is performed. In the case of the EMI filter undamped, in the vicinity of the resonant frequency the correction factor contains a pair of complex poles, and also a pair of right half-plane complex zeroes that cause a "glitch" in the magnitude plot of the correction factor. Instead in the second case, with the damped filter is possible to see that the transfer function is practically unchanged, there is a very little variation,

therefore we can expected that the performances will not be influenced by the presence of the input filter.

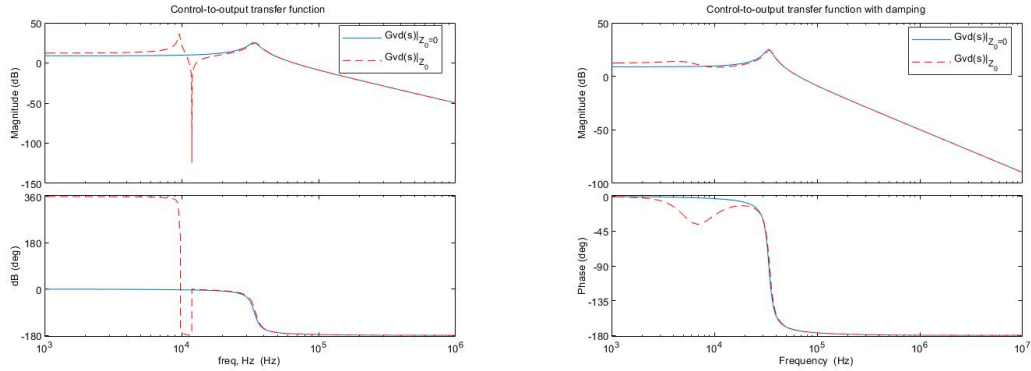


Figure 4.13: Comparison between $G_{vd}(s)$ without input filter and $G_{vd}(s)$ with input filter undamped. **Figure 4.14:** Comparison between $G_{vd}(s)$ without input filter and $G_{vd}(s)$ with input filter damped.

4.1.2 Filter components final values

The final values of the component of the input filter was chosen taking into consideration cost and dimension, comparing the couples C_f ad L_f that provide the same attenuation.

The values chosen to have a compromise between the two figures of merit are $C_f = 150\mu F$ and $L_f = 180\mu H$. The value for the optimum damping involves $R_f = 86m\Omega$ and $C_f = 37mF$. That is clearly a too big value, therefore for reducing this quantity at the expense of a small impact on the control-to-output function a $R_f = 1\Omega$ and $C_f = 300\mu F$ can be chosen.

The wanted attenuation for the current to comply with standards limits is 127 dB, that is exactly the attenuation obtained with the filter.

- Stability

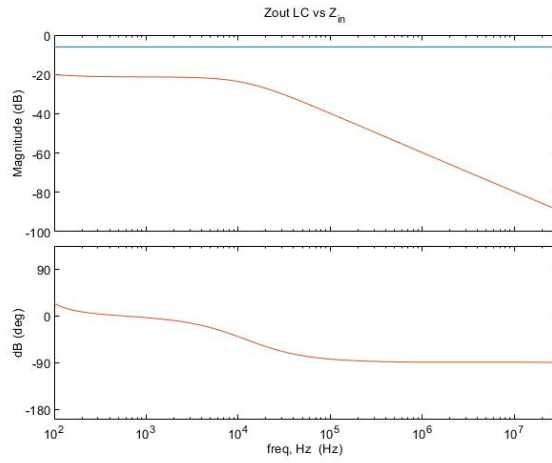


Figure 4.15: Comparison between output impedance of the LC filter and input impedance of the converter.

- Performance

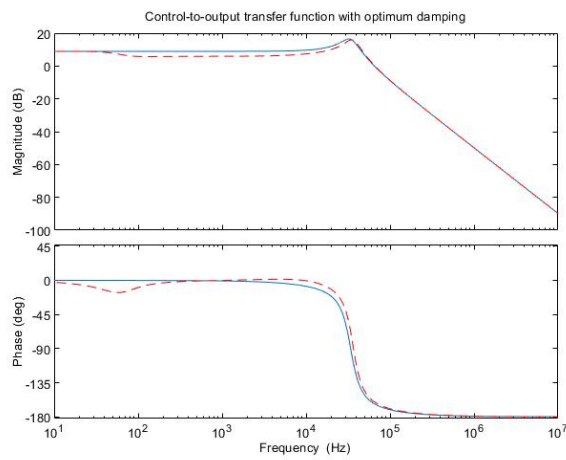


Figure 4.16: Comparison between control to output transfer function of the system with and without input filter.

- Attenuation

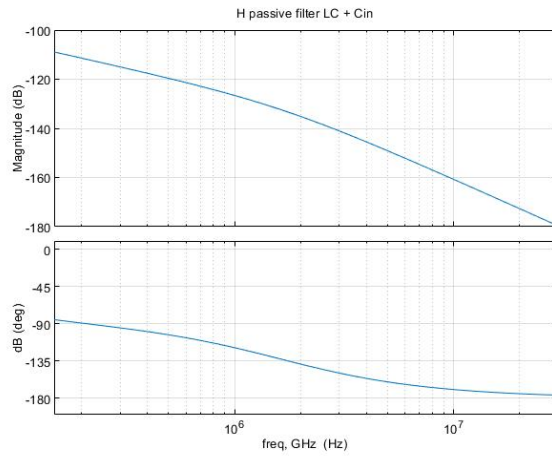


Figure 4.17: Transfer function of the current from the noise current source due to the buck converter to the LISN.

Finally comparing the CISPR average and quasi-peak limits with the spectrum of the DM voltage at the LISN, obtained with the insertion of the LC filter, it's possible to see that the peak at the fundamental is below the required standard.

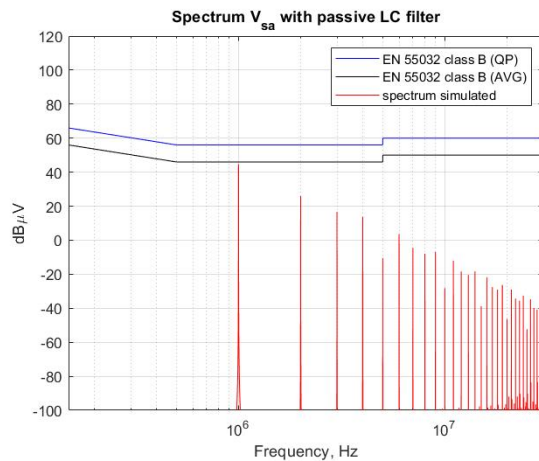


Figure 4.18: Spectrum of DM voltage compared with CISPR limits.

4.2 π -filter

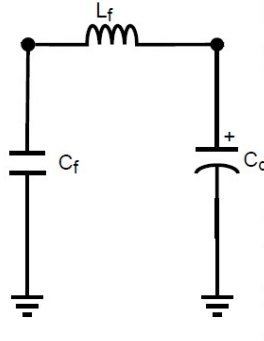


Figure 4.19: Schematic of π filter.

For the realization of the π -filter the same work flow of the previous solution was followed. The voltage attenuation is computed with the following equation:

$$\frac{V_{out,filter}(s)}{V_{in,filter}(s)} = \frac{1}{1 + s^2 L_f C_f} \quad (4.20)$$

and the corner frequency is given by:

$$f_c = \frac{1}{2\pi\sqrt{L_f C_f}} \quad (4.21)$$

since we have the voltage transfer function with a slope of 40dB/dec, in order to set properly the corner frequency the following equations must be observed:

$$A_{dm} = \left(\frac{f_{sw}}{f_c}\right)^2 \quad \rightarrow \quad A_{dm}[dB] = 40 \log\left(\frac{f_{sw}}{f_c}\right) \quad (4.22)$$

$$f_c = \frac{f_{sw}}{10^{A_{dm}[dB]/40}} \quad (4.23)$$

The attenuation is then recomputed considering the effect of the LISN and the different couples of capacitor and inductor that provide the same attenuation are obtained.

Now the damping is evaluated following the two different approach:

- with a reduction of the output impedance of the filter applying a resistor in parallel with the damping capacitor. The inductor used has a value of $L_f = 680nH$ while the capacitor is $C_f = 28\mu F$, instead to ensure stability and also performance unchanged a damping resistor of $75m\Omega$ and a damping capacitor of $178\mu F$ are required. In this case using only the effect of the damping to reduce the value of the peak of the output impedance of the filter falls into a too big and expensive capacitive solution.

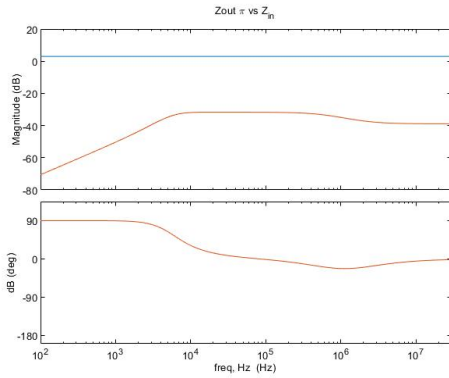


Figure 4.20: $Z_{out,\pi}$ with damping compared with $Z_{in,buck}$.

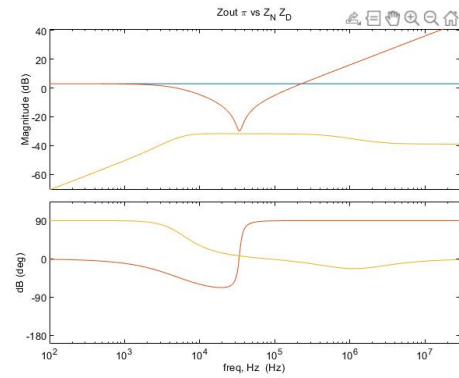


Figure 4.21: $Z_{out,\pi}$ with damping compared with Z_N and Z_D

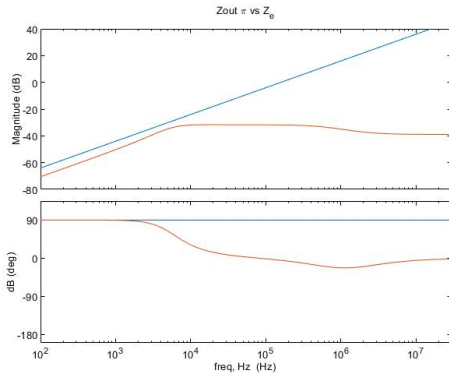


Figure 4.22: $Z_{out,\pi}$ with damping compared with Z_e .

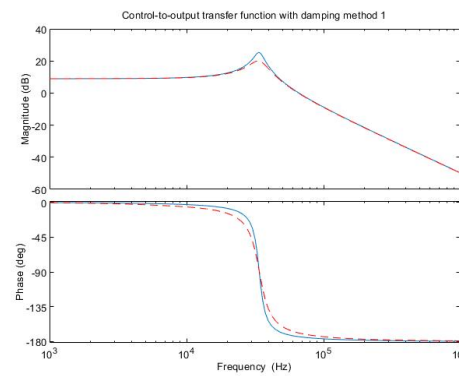


Figure 4.23: Comparison between control to output transfer function with and without input filter.

- with the other approach the filter resonant frequency is kept away from the crossover frequency of the converter. In this case the components used are $C_f = 188\mu F$ and $L_f = 100nH$, with a damping capacitor of $19\mu F$ and a damping resistor of $230m\Omega$. In this case the damping values are reduced but there is an increase on the value of C_f .

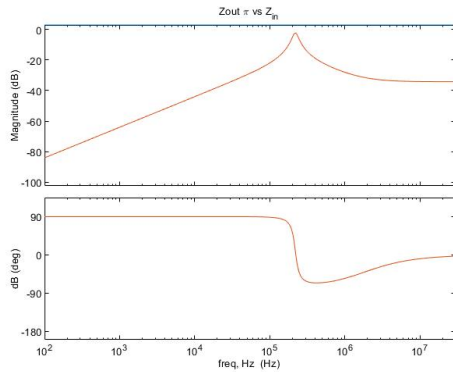


Figure 4.24: $Z_{out,\pi}$ with damping compared with $Z_{in,buck}$.

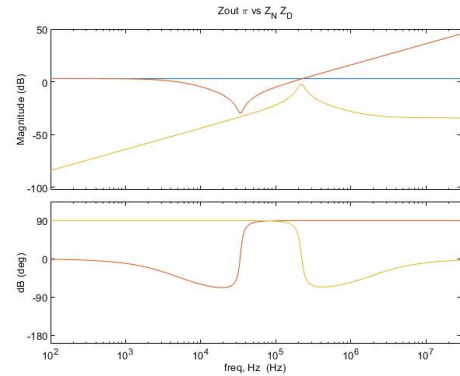


Figure 4.25: $Z_{out,\pi}$ with damping compared with Z_N and Z_D

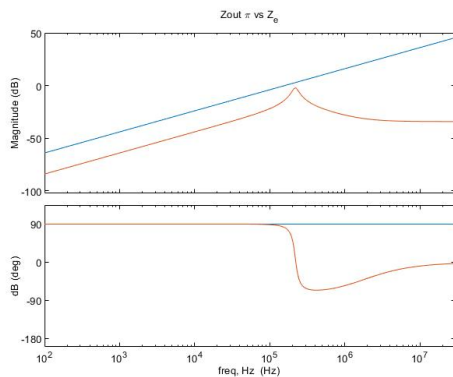


Figure 4.26: $Z_{out,\pi}$ with damping compared with Z_e .

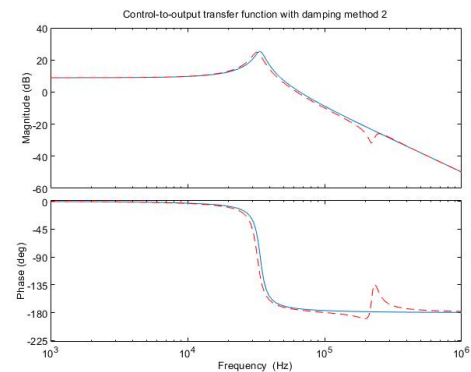


Figure 4.27: Comparison between control to output transfer function with and without input filter.

Therefore an approach in the middle of the two possible solutions is followed. The obtained values are: $L_f = 470nH$ and $C_f = 40\mu F$, for the damping the values required are: $R_d = 250m\Omega$ and $C_d = 22\mu F$, using the real component an electrolytic capacitor with an ESR of $250m\Omega$ and a capacitance of $47\mu F$ is selected.

- Stability

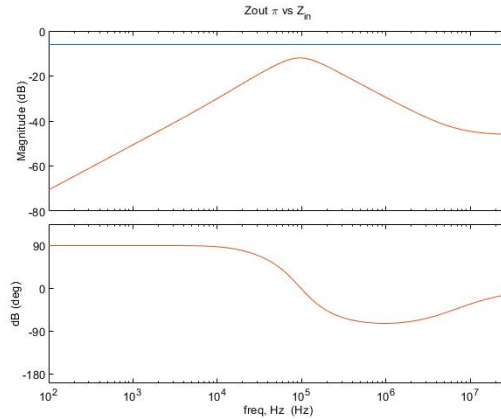


Figure 4.28: Comparison between output impedance of the π filter and input impedance of the converter.

- Performance

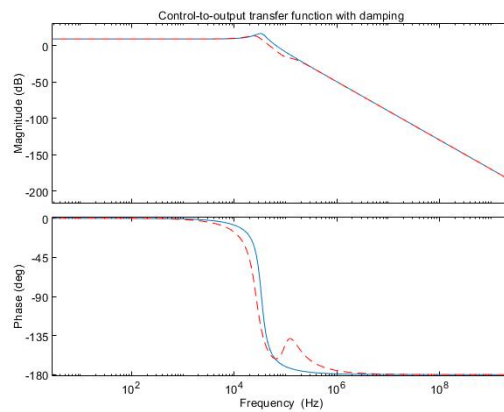


Figure 4.29: Comparison between control to output transfer function of the system with and without input filter.

- Attenuation

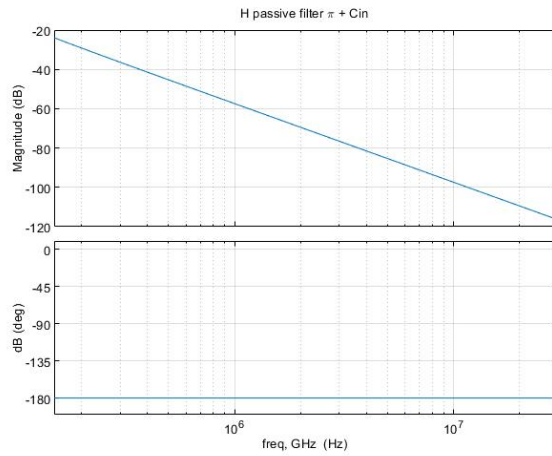


Figure 4.30: Transfer function of the voltage from the noise source due to the buck converter to the LISN.

Reaching the wanted attenuation of -58dB for disturbance voltage. Subsequently the CISPR average and quasi-peak limits and the spectrum of the DM voltage at the LISN, with the presence of the π -filter are compared, obtaining an effective reduction of the emission peak level of the desired value.

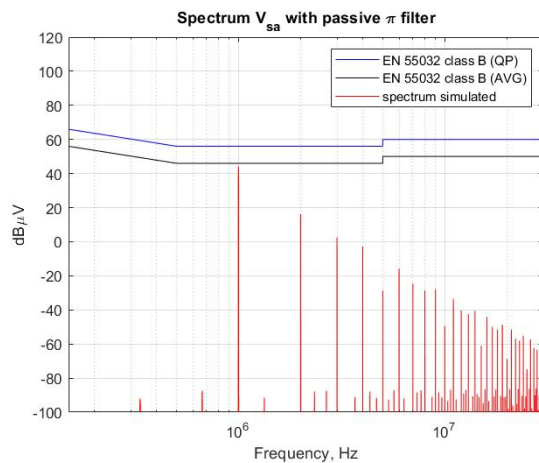


Figure 4.31: Spectrum of DM voltage compared with CISPR limits.

4.3 Comparison between LC and π filter

The values of the components found for the different filter topologies are substantially different. Indeed computing the transfer function between the input and output current of the two studied filter is possible to see a difference in the attenuation value. The LC filter attenuates current with a slope of 40 dB/dec, instead π filter attenuate current with a slope of 60 dB/dec.

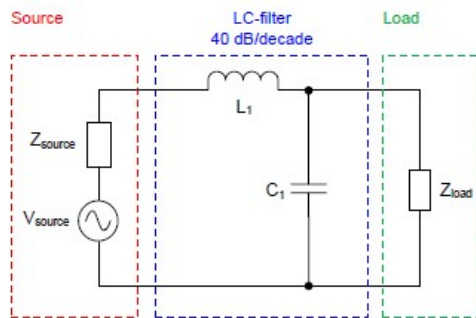


Figure 4.32: LC filter topology.

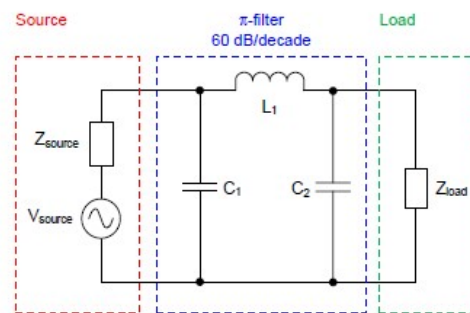


Figure 4.33: π filter topology.

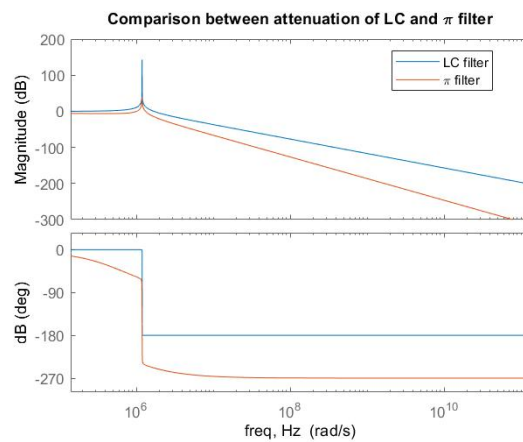


Figure 4.34: Transfer function of LC filter and π filter.

To obtain the same attenuation the cutoff frequency of the two filter is different. Since the required current attenuation is approximately 120dB at 1MHz, the resonant frequency for the π -filter should be two decade below, instead for the LC filter is required a cutoff frequency lower than about three

decade.

This implies a different choice in the components value that results in smaller dimension and lower cost for the π -filter.

The π -filter topology is the one on which the subsequent analysis of the active filter is based, starting from the found values of the components of this passive solution, smaller dimension can be achieved due to the enhanced value of the capacitor determined by the active filter.

Chapter 5

Active filter

5.1 Active filter topologies

The passive EMI filtering technique is the direct and commonly used approach to reduce the conducted emissions of a power electronic circuit, although the cost, size and weight of the passive filter components cause significant limitations in some applications.

On the other hand, for the AEF technique active devices are used to detect the residual noise and inject an opposite noise that directly attenuates the EMI current measured at the input. Its operation is based on the superposition theorem of signals with equal amplitude and opposite phase: the injected current or voltage ideally cancels the incident input ripple current or voltage contribution from the EMI source. Practically the current ripple will be reduced sufficiently to meet the EMC requirements, expecting a reduction in size and cost compared to an equivalent passive design.

There are different active-filter topologies classified according to the sensed noise parameter and the way the cancellation signal is injected. The active control technique are classified as follows:

- Voltage sense (VS) or current sense (CS)
- Voltage injection (VI) or current injection (CI)
- Feedback (FB) control or a feedforward (FF) control structure.

In Figure 5.1 the various realizations of the AEF are represented, in particular Z_S is the equivalent noise source impedance, Z_L is the impedance of the noise receiver for EMI measurements that in this case is the line impedance stabilization network (LISN) and A represents the gain of the active circuit.

Voltage injection designs use a controlled series voltage source to hinder the flow of the noise current to the LISN, instead *current injection* designs employ a controlled shunt current source to compensate the noise current induced by the noise source.

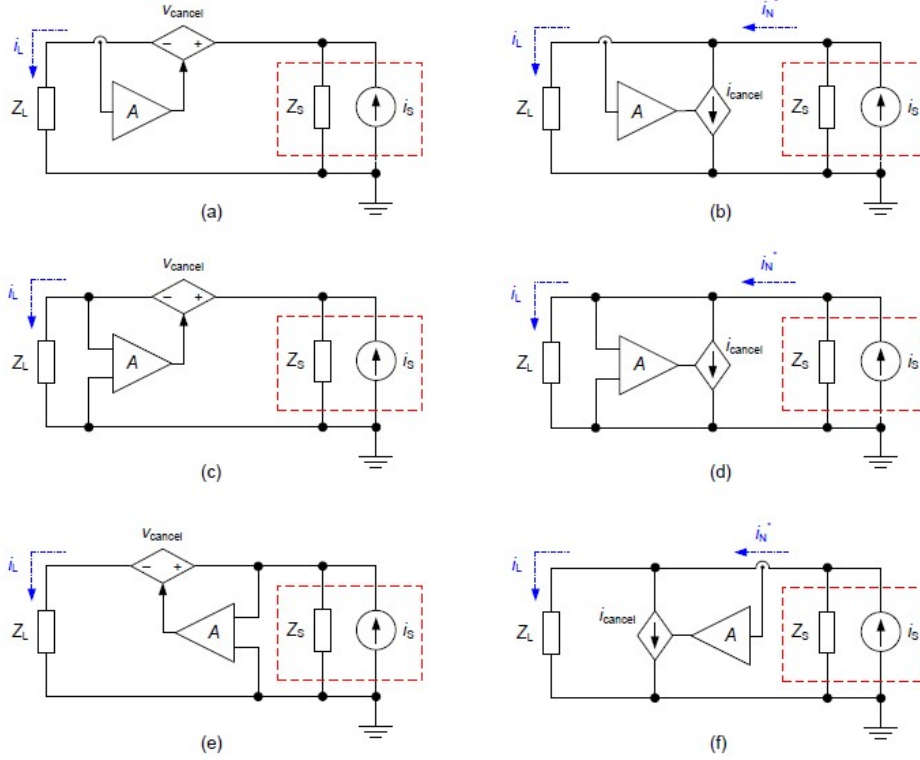


Figure 5.1: Different topologies of active filter [26].

From the point of view of control a distinction between *feedback* design and *feedforward* one can be done. In the first case the residual noise is sensed to the side of the LISN and the opposite signal is injected, with high gain, back to it. In the second case the disturbance is sensed at the noise source and the signal is injected with unitary gain at the side of the load [27].

The most appropriate topology for the type of applications studied in this thesis is the VSCI that does not require the use of additional magnetic components, that are ordinarily large and can cause an increase in volume and cost.

5.2 Active filter design

Considering the previous analysis on the different topologies of active filter the one implemented for the converter analyzed, senses the voltage at LISN side and injects a cancellation current into it. The same final attenuation of the π -filter is achieved with the difference that for the active one a smaller value of components can be used. This is possible due to the fact that the value of the final capacitance ideally turns out to be the value of the effective capacitance enhanced by a factor G_{op} , using the stage of the operational amplifier as capacitive multiplier.

As can be seen in Figure 5.2, the capacitance of the π -filter can be replaced with the active one obtaining the same attenuation in the two cases, equaling C_F and $C_{inj} \cdot G_{op}$.

As a first approximation the multiplication factor G_{op} can be expressed as:

$$G_{op} \approx \frac{C_{SEN}}{C_{AEFC}} \quad (5.1)$$

obtaining a final value for the replaced capacitance equal to:

$$C_{eq} \approx \frac{C_{SEN}}{C_{AEFC}} \times C_{INJ} \quad (5.2)$$

achieving the same attenuation of the π -filter substituting the expression of C_{eq} in the following equation:

$$\frac{V_{out,filter}(s)}{V_{in,filter}(s)} = \frac{1}{1 + s^2 L_{in} C_{eq}} \quad (5.3)$$

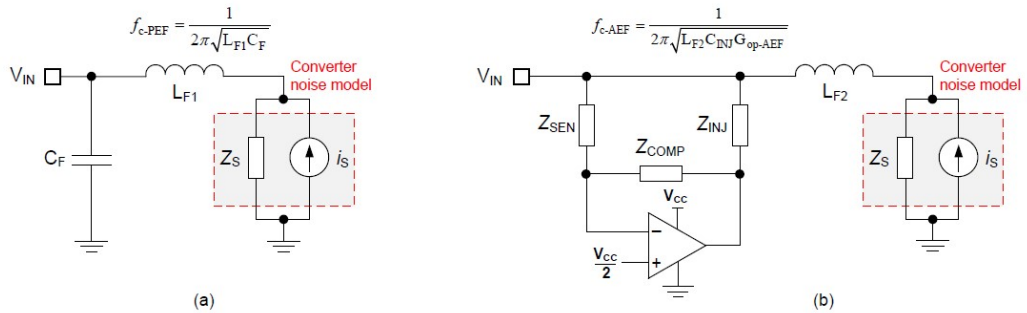


Figure 5.2: Transformation from π -filter to active filter [28].

The value of G_{op} , that is the closed loop gain, can also be written as:

$$G_{op} = -\frac{A_v \frac{Z_{COMP}}{Z_{COMP}+Z_{SEN}}}{1 + A_v \frac{Z_{SEN}}{Z_{COMP}+Z_{SEN}}} \quad (5.6)$$

hence the ratio between Z_{COMP} and Z_{SEN} is given by:

$$\frac{Z_{COMP}}{Z_{SEN}} = \frac{(1 + A_v)G_{op}}{-A_v - G_{op}} \quad (5.7)$$

In this analysis then, the non-idealities of the operational amplifier were taken into consideration: the value of A_v is not considered infinite and constant, the input resistance R_{in} has not an infinite impedance and the output resistance R_{out} has a value different from zero. Therefore the new expression for G_{op} can be written as:

$$G_{op''} = -\frac{A_v \frac{Z_{COMP}}{Z_{COMP}+Z_{SEN}} \cdot \frac{(R_{in} // Z_{SEN} + Z_{COMP}) // Z_{INJ}}{(R_{in} // Z_{SEN} + Z_{COMP}) // Z_{INJ} + R_{out}}}{1 + A_v \frac{Z_{SEN}}{Z_{COMP}+Z_{SEN}} \cdot \frac{(R_{in} // Z_{SEN} + Z_{COMP}) // Z_{INJ}}{(R_{in} // Z_{SEN} + Z_{COMP}) // Z_{INJ} + R_{out}}} \quad (5.8)$$

where A_v is:

$$A_v = \frac{A_{v0}}{\left(1 + \frac{s}{s_{p1}}\right)\left(1 + \frac{s}{s_{p1}}\right)} \quad (5.9)$$

so as the equivalent impedance is obtained:

$$Z_{eq} = (R_{in} // \frac{Z_{COMP}}{1 + A_v} + Z_{SEN}) // \frac{Z_{INJ}}{1 + G_{op''}} \quad (5.10)$$

and the final attenuation can be computed.

Finally the stability of the op amp can be verified considering the following schematic:

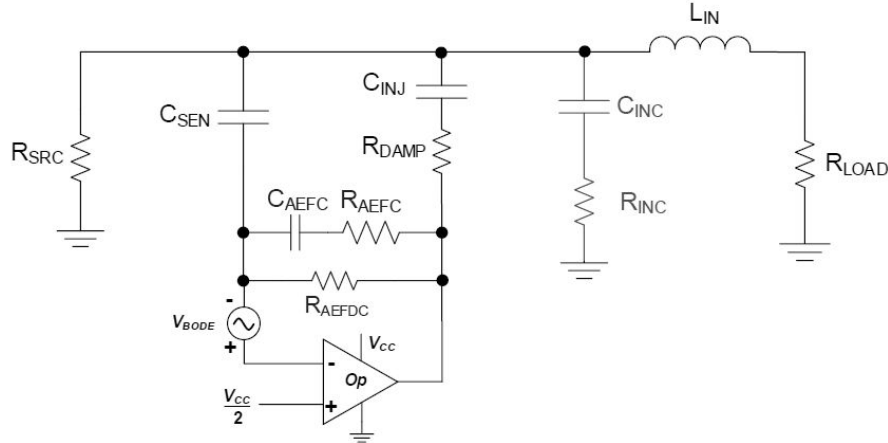


Figure 5.4: Schematic for the analysis of closed loop [29].

and implementing the subsequent equations:

$$T = A_v \beta \quad (5.11)$$

where the term β is given by:

$$\beta = \frac{Z_{INJ}}{Z_{INJ} + Z_0} \frac{Z_{SEN}}{Z_{COMP} + Z_{SEN}} + \frac{Z_0}{Z_{INJ} + Z_0} \quad (5.12)$$

$$Z_0 = (R_{LOAD} + L_{IN}) // \left(\frac{1}{sC_{INC}} + R_{INC} \right) // R_{SRC} \quad (5.13)$$

$$R_{LOAD} = \left(R_{buck} // \frac{1}{sC_{in}} // \left(\frac{1}{sC_d} + R_d \right) \right) \quad (5.14)$$

For the practical realization of the AEF the same value of inductor of the π filter ($L_f = 470nH$) is used. The value of the inductor is limited by the output current of the op amp, in fact the minimum value of the output current is given by:

$$i_{op\ amp} = \frac{v_{bare}}{Z_{L,inductor}} \quad (5.15)$$

where v_{bare} is the voltage level at the fundamental switching frequency.

For the choice of the operational amplifier used in the project an analysis of the one used in the LM25149-Q1 [30] automotive synchronous buck DC/DC controller produced by TI was performed.

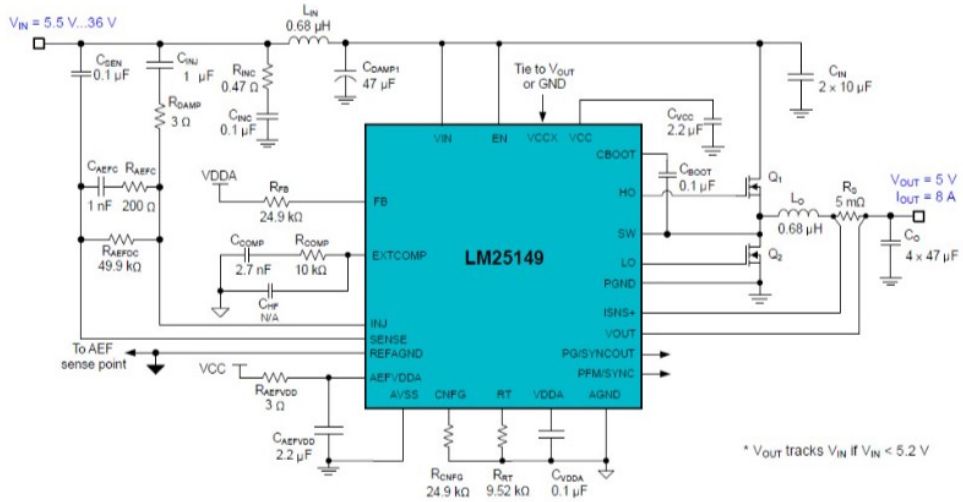


Figure 5.5: LM25149 Buck Regulator

The voltage at the input (V_{SENSE}) and at the output (V_{INJ}) of the op amp are simulated and the FFT is computed. By comparing the corresponding peaks at different frequency, the value of the closed loop gain was obtained and inverting equation 5.8 it is possible to derive the value of A_v .

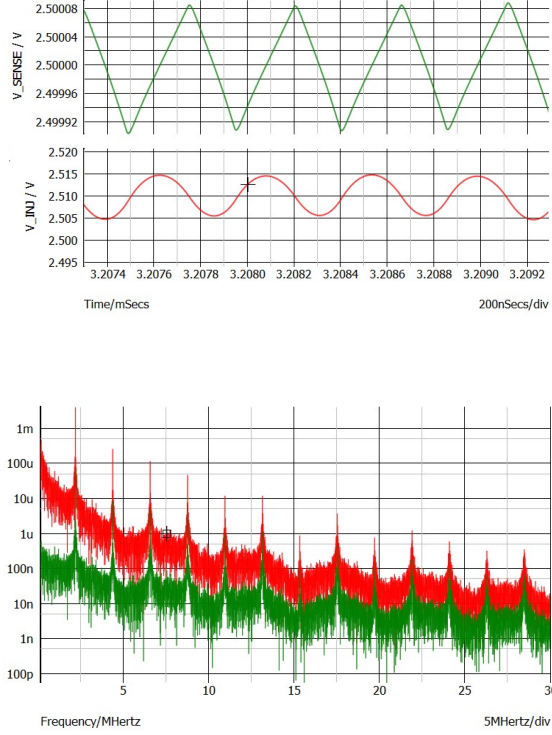


Figure 5.6: Simulation of V_{SENSE} and V_{INJ} of LM25149 and respective FFT.

Thus the op amp used for the design of the AEF, considering an R_{OUT} equal to 1Ω , has a GBW of 180MHz. Instead the required output current sourced and sunk by the op amp is approximately 50mA.

In the design of the project a G_{op} equal to 690 is chosen and the values obtained for guarantee a sufficient damping and the required attenuation are C_{INJ} equal to 680nF and R_{damp} equal to 2.55Ω . This leads to a ratio $\frac{Z_{COMP}}{Z_{SEN}}$ equal to 133, from which component values can be chosen, obtaining $C_{SEN} = 33nF$, $C_{AEFC} = 10nF$ and $R_{AEFC} = 650\Omega$.

Selecting the real components and considering also the parasitic effects, the ESR are added in the project and the final schematic obtained is represented in Figure 5.7

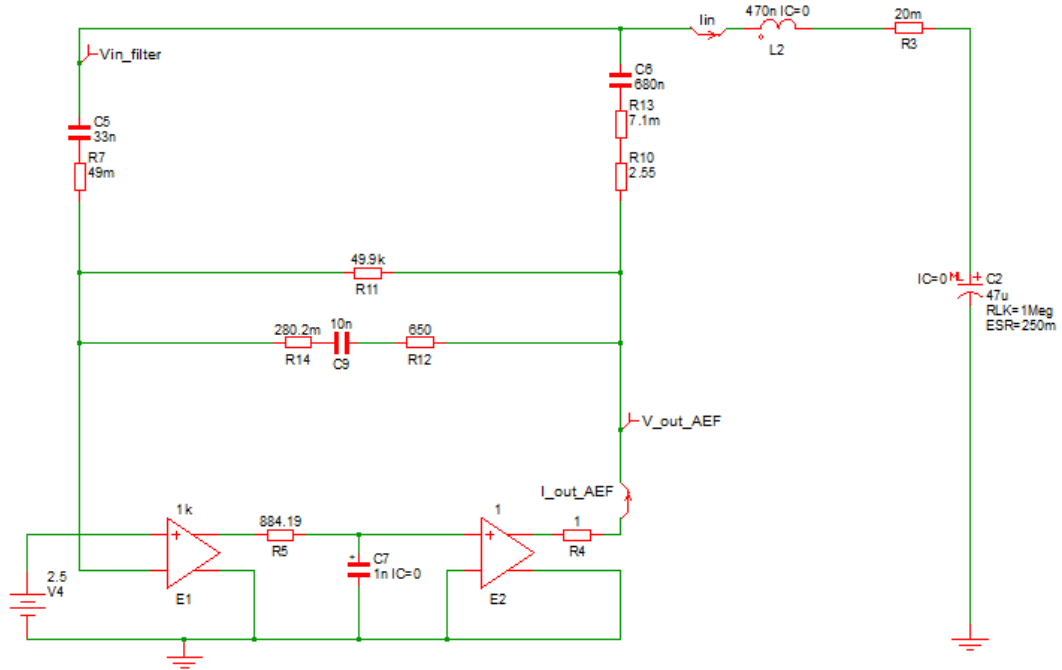


Figure 5.7: Final schematic of the AEF with real components.

At this point the stability analysis is performed, the computed loop gain is reported in Figure 5.8. The stability at low frequency is guaranteed by the component C_{AEFC} , R_{AEFC} and R_{AEFDC} .

Instead if also a second pole of the operational amplifier is considered, instability may occur. Evaluating the case of a simple operational amplifier used for the analyzed application with the second pole at 50 MHz, the new loop gain obtained is pictured in Figure 5.9. It can be noted that the presence of the second pole of the operational amplifier causes a reduction in the value of phase margin.

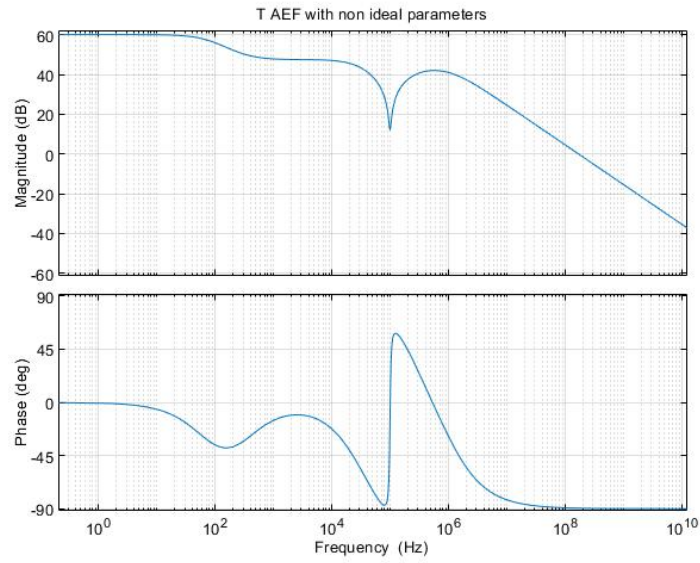


Figure 5.8: Computation of the loop gain of the AEF.

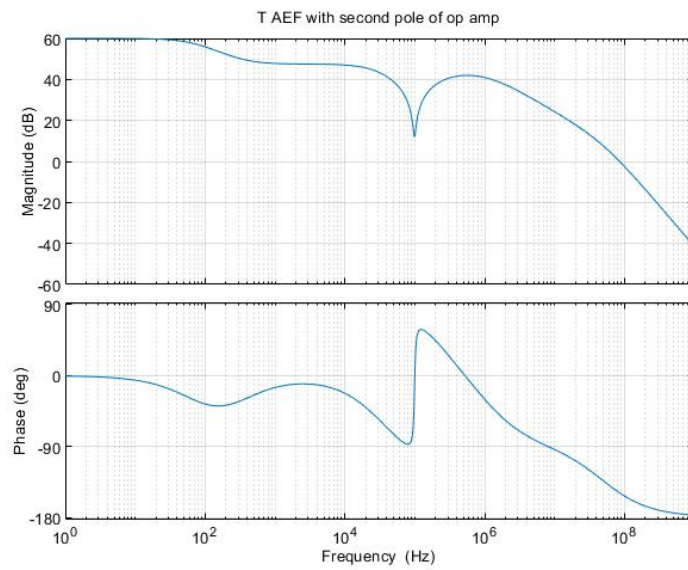


Figure 5.9: Computation of the loop gain of AEF without C_{INC} and R_{INC} with operational amplifier with a second pole.

The components C_{INC} and R_{INC} intervene in order to achieve a phase margin of about 60° .

At high frequency β can be approximated as:

$$\beta \approx \frac{Z_0}{Z_{INJ}} \quad (5.16)$$

so as to have a remarkable effect of the added component the predominant term in the expression of Z_0 (5.13) should be the series of C_{INC} and R_{INC} . Therefore at high frequency the impedance of this component must be much lower than the impedance of the inductor. If this constraint is satisfied β becomes:

$$\beta \approx \frac{Z_{INC}}{Z_{INJ}} \quad (5.17)$$

as can be seen in the following figure the whole expression of the loop gain and the approximated one are equal at high frequency:

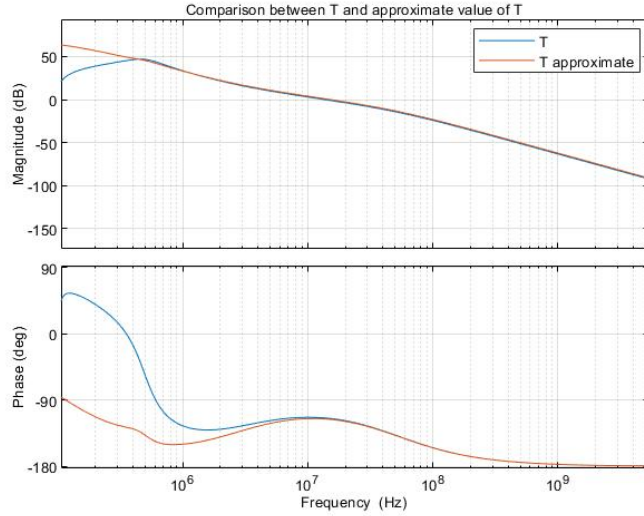


Figure 5.10: Comparison between whole expression of loop gain and approximated one, at high frequency.

Consequentially the expression of β is equal to:

$$\beta = \frac{C_{INJ}}{C_{INC}} \frac{1 + sC_{INC}R_{INC}}{1 + sC_{INJ}R_{INJ}} \quad (5.18)$$

introducing a zero at a frequency equal to $f_z = \frac{1}{2\pi C_{INC} R_{INC}}$ that has to be about one decade before the 0dB crossing of the loop gain, in order to have the maximum value of the phase variation due to the zero in correspondence of the crossing of the horizontal axis.

However in the expression of β also a pole is present at a frequency equal to $f_p = \frac{1}{2\pi C_{INJ} R_{INJ}}$, it follows that the position of the zero should be close enough to the pole in order to not let the phase decrease excessively.

With these constraints the values are chosen to be equal to: $C_{INC} = 200nF$ $R_{INC} = 300m\Omega$. The new loop gain is depicted in Figure 5.12, and as can be seen the phase margin is equal to approximately 60° .

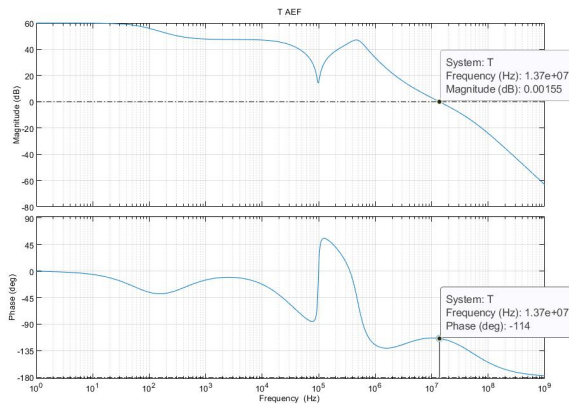


Figure 5.11: Computation of phase margin of the final loop gain.

The same result is also obtained with simulation:

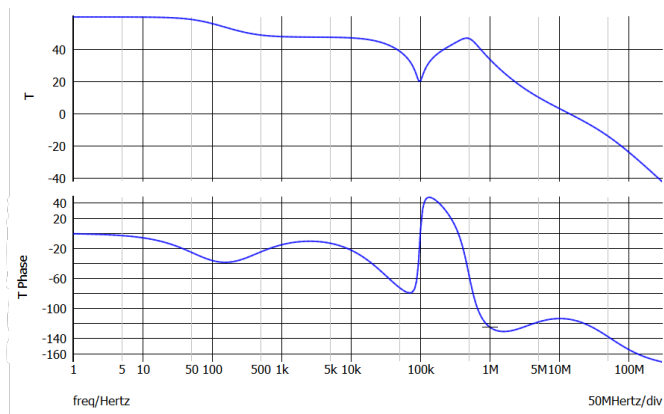


Figure 5.12: Simulation of the final loop gain.

The subsequent analysis carried out is about the interaction between the active filter and the converter. The output impedance of the AEF is compared to the input impedance of the buck converter and since the value of Z_{OUT} of the filter is lower than the value of Z_{IN} of the converter, stability is ensured. Instead to investigate how the control-to-output transfer function $G_{vd}(s)$ is altered the comparison between the output impedance of the filter and Z_N and Z_D is done. Achieving a small variation on the final $G_{vd}(s)$ function thanks to the proper damping of the filter. Afterwards to ensure that the output impedance of the converter is not heavily affected by the filter the output impedance of the filter is compared with Z_e .

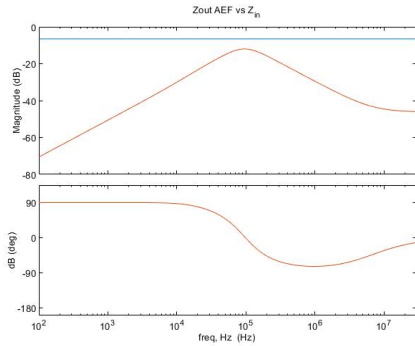


Figure 5.13: Comparison between Z_{OUT} filter and Z_{IN} converter.

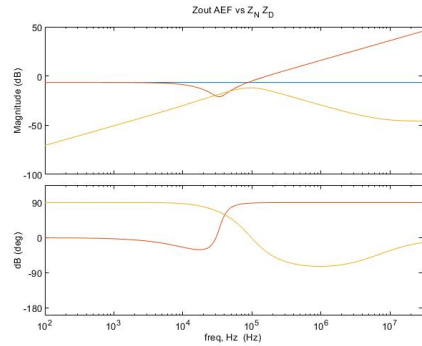


Figure 5.14: Comparison between Z_{OUT} filter and Z_N and Z_D .

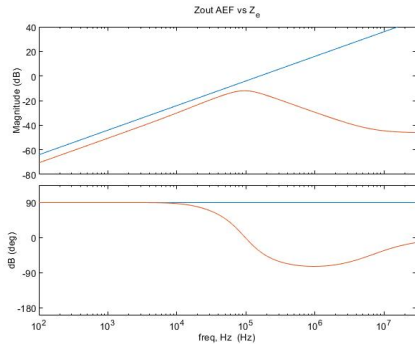


Figure 5.15: Comparison between Z_{OUT} filter and Z_e .

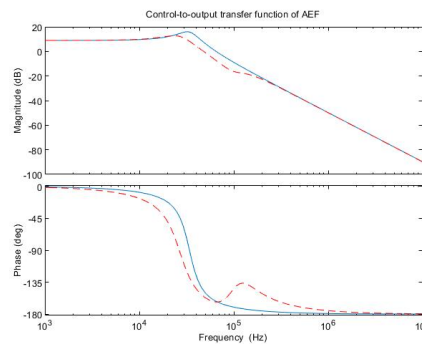


Figure 5.16: Comparison between $G_{vd}(s)$ with filter and without filter.

The equivalent impedance is then computed and simulated and it is verified that at the switching frequency the value of the impedance is the one wanted. At 1MHz the equivalent impedance has a value of about $-48dB\Omega$ that correspond to a value of a capacitor equal to $40\mu F$, that is the initial value of the capacitor of the π -filter.

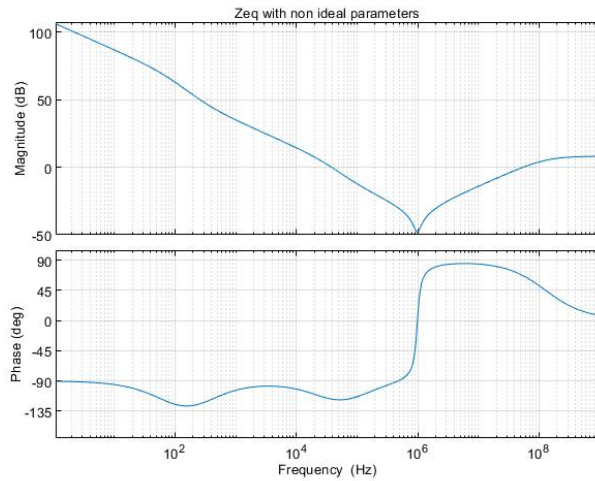


Figure 5.17: Computation of the equivalent impedance of the AEF with parasitic effect and non ideality of op amp.

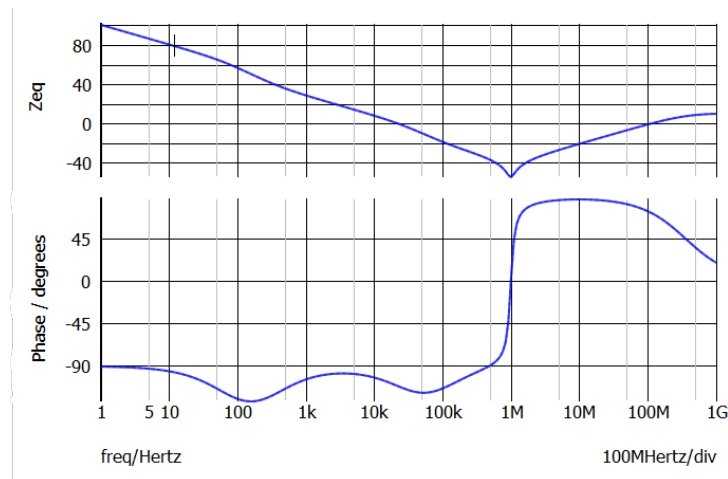


Figure 5.18: Simulation of the equivalent impedance of the AEF with parasitic effect and non ideality of op amp.

The complete analysis can be now performed putting together the LISN for measuring the level of conducted disturbance, the AEF and the buck converter configured to provide the highest value of disturbance.

The entire schematic is represented in Figure 5.19.

In Figure 5.20 the waveforms of the simulation are depicted. I_{BUCK} represents the trapezoidal input current of the buck converter that is the cause of the EMI problems. It determines $V_{IN,ripple}$, the voltage ripple to attenuate in order to comply with the regulation. Consequentially the current $I_{OUT,AEF}$ is injected by the op amp to compensate completely or almost completely the inductor ripple current. And only the residual of this current flows in the line of voltage source, therefore on the LISN the remaining voltage ripple that is observed is of the order of few μV .

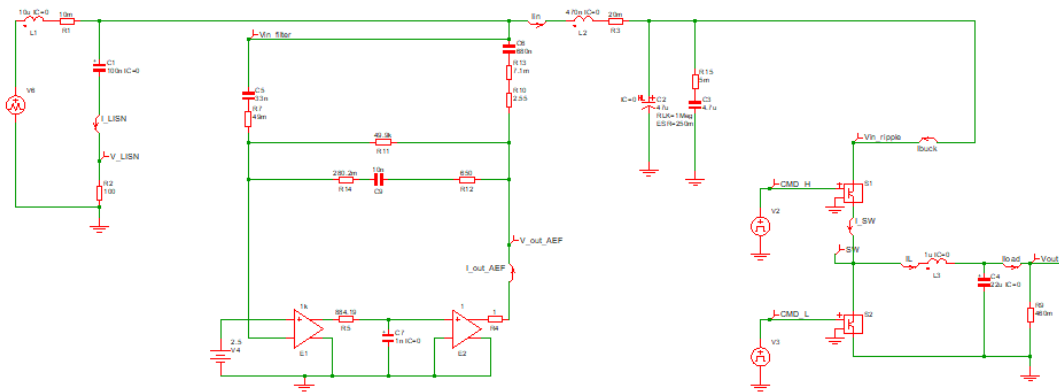


Figure 5.19: Schematic of the whole system with LISN, active EMI filter and buck converter.

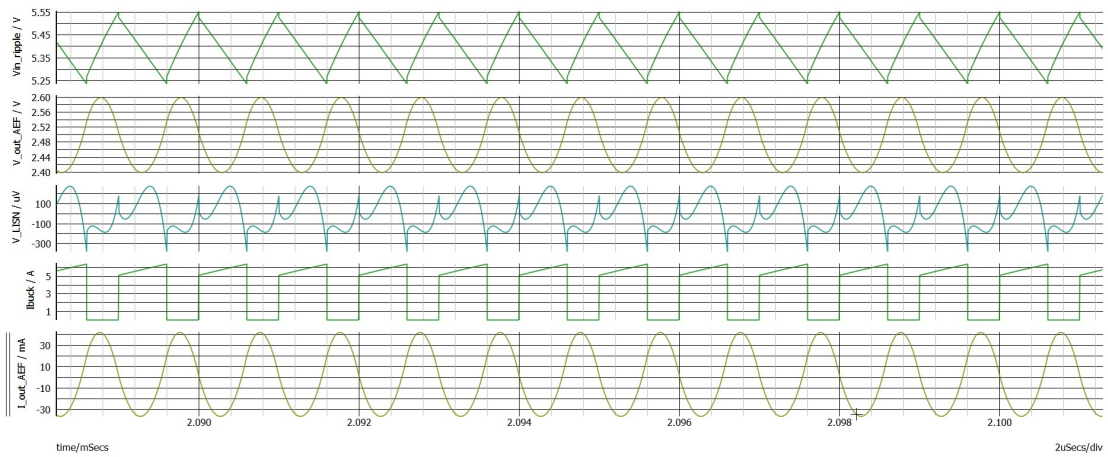


Figure 5.20: AEF simulated waveforms.

Finally the value of the attenuation can be computed:

$$Att = \frac{Z_{O,LISN} // Z_{eq,AEF}}{Z_{O,LISN} // Z_{eq,AEF} + Z_L} \frac{R_{LISN}}{R_{LISN} + \frac{1}{sC_{LISN}}} \quad (5.19)$$

obtaining the desired 58dB of attenuation at 1Mhz (Figure 5.21) and it is also verified with simulation (Figure 5.22).

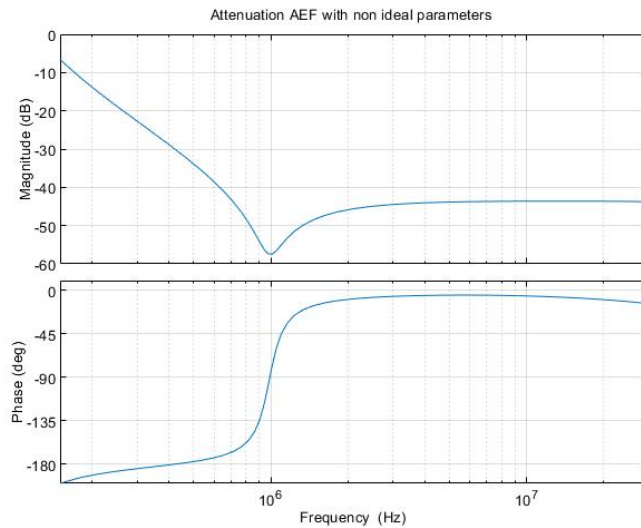


Figure 5.21: Computation of the attenuation of the AEF.

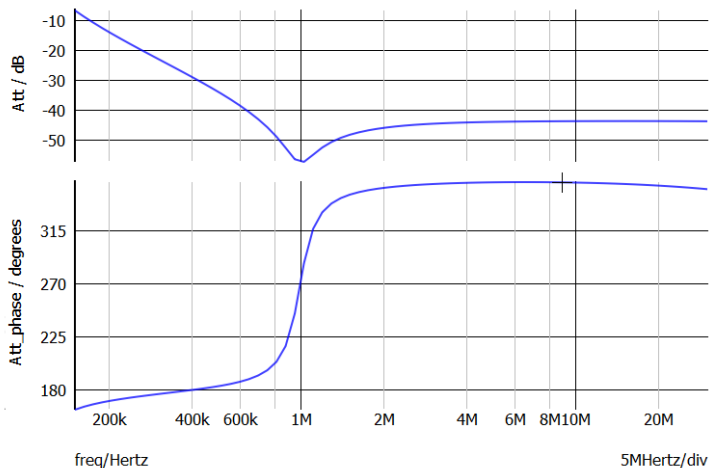


Figure 5.22: Simulation of the attenuation of the AEF.

The FFT is then evaluated and compliance with standards is verified, obtaining the peak at the fundamental frequency lower than the standard requirement.

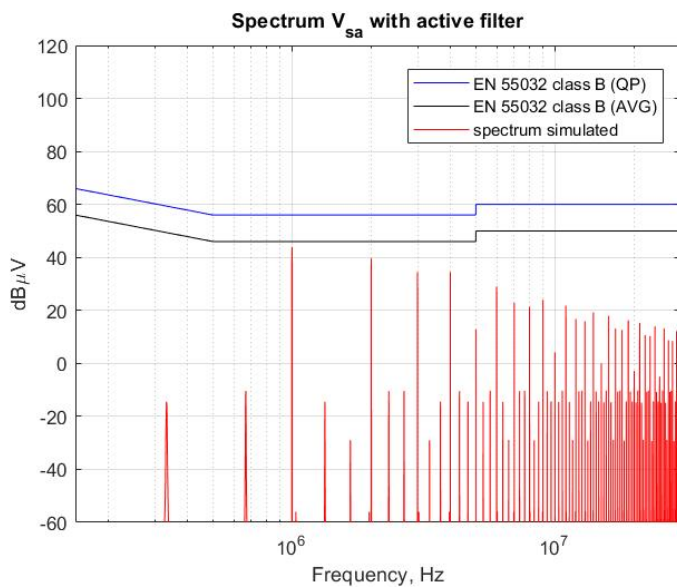


Figure 5.23: Spectrum of the voltage at the LISN compared with the CISPR standard regulation.

5.3 Comparison between AEF and π -filter

The passive π -filter and the active one have been realized in order to behave in the same way at the switching frequency. Using the same values for the inductor and the damping in the two solutions implemented, and replacing the capacitor C_f of the π -filter with the AEF.

It is therefore possible to emphasize the same behaviour at the frequency of interest between the capacitor of the filter and the active implementation. Obtaining an equivalent final attenuation of the peak of conducted emissions in both cases.

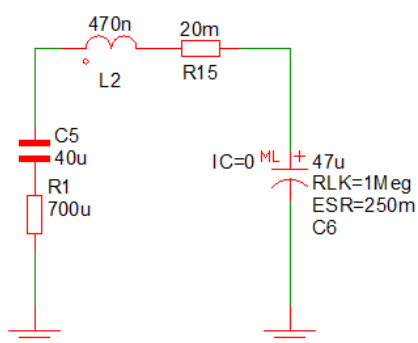


Figure 5.24: Schematic of π -filter.

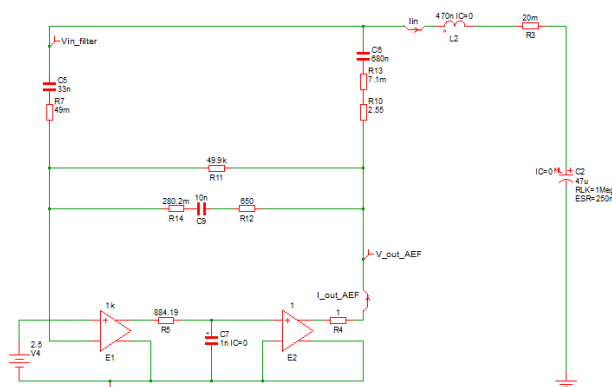


Figure 5.25: Schematic of AEF.

In the following figures the equivalent behavior of the passive and active solution can be observed.

In particular the equivalent impedance of the active filter is equal to the equivalent impedance of the passive filter capacitor at 1 MHz as depicted in Figure 5.26.

While in Figure 5.27 the same value of attenuation at the switching frequency in the two different solutions can be noticed.

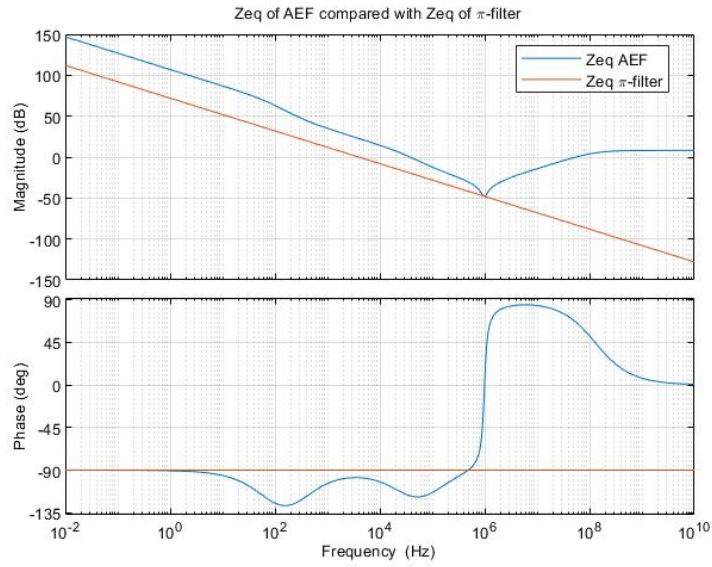


Figure 5.26: Comparison between equivalent impedance of active and passive filter.

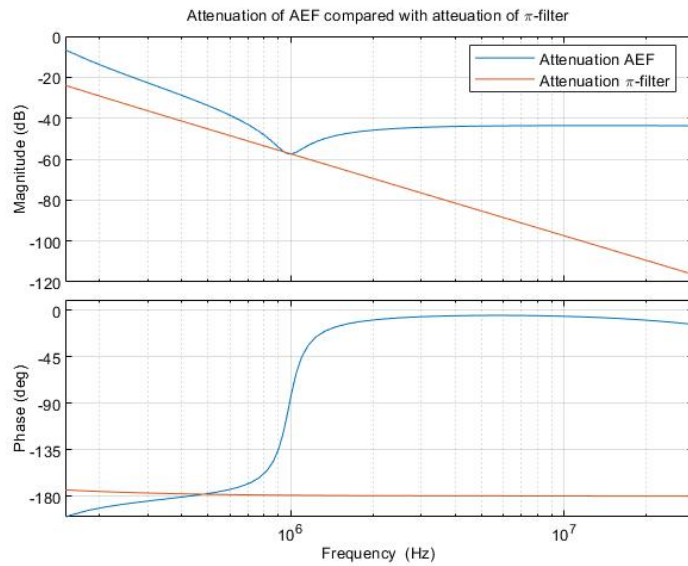


Figure 5.27: Comparison between attenuation of active and passive filter.

Even if the behaviour at the switching frequency is equal and both filter attenuate the level of conducted emission of the same quantity, there are several advantages using the active solution.

The most noteworthy advantage is the reduction of dimension in area and volume. Using the same inductor for both solution the values obtained are reported in the following.

For the passive filter:

π -filter	value	footprint	height
L_f	0.470 μ H	7.8 mm^2	1 mm
C_f	40 μ F	44.1 mm^2	1.35 mm

obtaining a total footprint equal to 51.9 mm^2 and a volume of 67.34 mm^3 .

For the active filter:

AEF filter	value	footprint	height
L_f	0.470 μ H	7.8 mm^2	1 mm
C_{INJ}	680nF	4.68 mm^2	1 mm
C_{AEFC}	10nF	2.08 mm^2	0.33 mm
C_{SENSE}	33nF	3 mm^2	0.6 mm
R_{AEFC}	650 Ω	3 mm^2	0.6 mm
R_{AEFDC}	49.9 $k\Omega$	3 mm^2	0.6 mm
R_{DAMP}	2.55 Ω	3 mm^2	0.6 mm

obtaining a total footprint equal to 26.56 mm^2 and a volume of 20.36 mm^3 .

Therefore the reduction in size is of the order of 50%, instead the reduction in volume is of the order of 70%.

What is achieved is a significant reduction in component dimension but at the same time maintaining the same level of noise reduction.

The same analysis can be performed also for the cost.
For the passive filter:

π -filter	value	price
L_f	0.470 μ H	0.11 \$
C_f	40 μ F	0.84 \$

obtaining a total cost of 0.95\$.
For the active filter:

AEF filter	value	price
L_f	0.470 μ H	0.11 \$
C_{INJ}	680nF	0.04 \$
C_{AEFC}	10nF	0.01 \$
C_{SENSE}	33nF	0.03 \$
R_{AEFC}	650 Ω	0.01 \$
R_{AEFDC}	49.9k Ω	0.01 \$
R_{DAMP}	2.55 Ω	0.01 \$

obtaining a total cost of 0.22\$. Also in this case a significant reduction around 75% is obtained.

Another notable difference concern the effect of the parasitic elements on the level of attenuation. Regarding the π -filter the value of the attenuation is decided by the value of the capacity alone (combined with the value of the inductor). Therefore a change in the value of the capacitance due to the parasitic component determines a big change in the value of the attenuation. On top of this, the value of the capacitor must be chosen with a small value of ESR but this increase the cost. On the other side a higher value of capacitor can be chosen, with a higher value of ESR, but in this case the increase of the value of component falls into an increase in size.

As can be seen in the following Figure even a variation of few $m\Omega$ in the value of ESR of the capacitor C_f leads to a variation on the attenuation level, making the device no longer compliant.

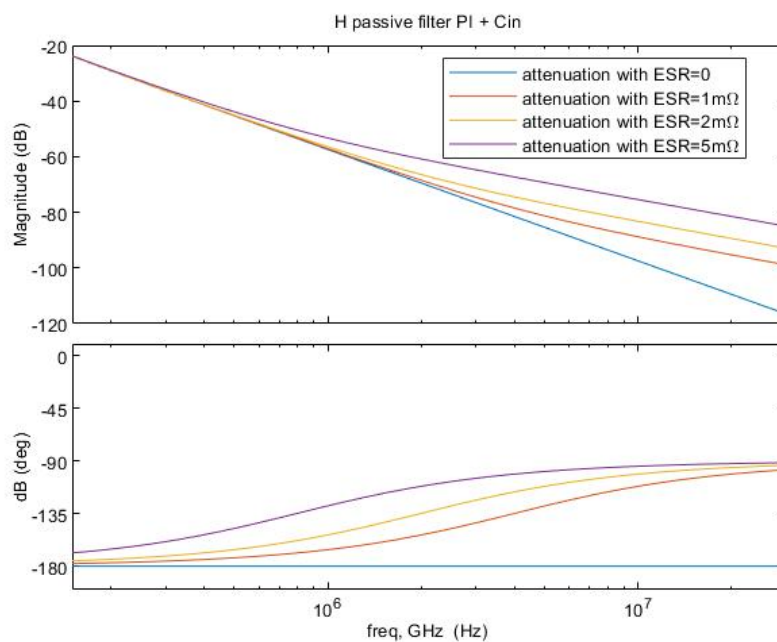


Figure 5.28: Comparison between attenuation of π -filter with variation of ESR of C_f .

On the contrary for the active filter solution the attenuation is given by a combination of ratio between the components value, therefore even if the capacitors present an high value of ESR the final value can be adjusted with the proper choice of capacitor in order to get the wanted ratio. In Figure 5.29 a variation of the ESR of the capacitors present in the AEF of the order of $100m\Omega$ determine a negligible variation on the level of attenuation. For the active filter therefore components with an high value of ESR can be chosen and this determine an advantage in term of total cost.

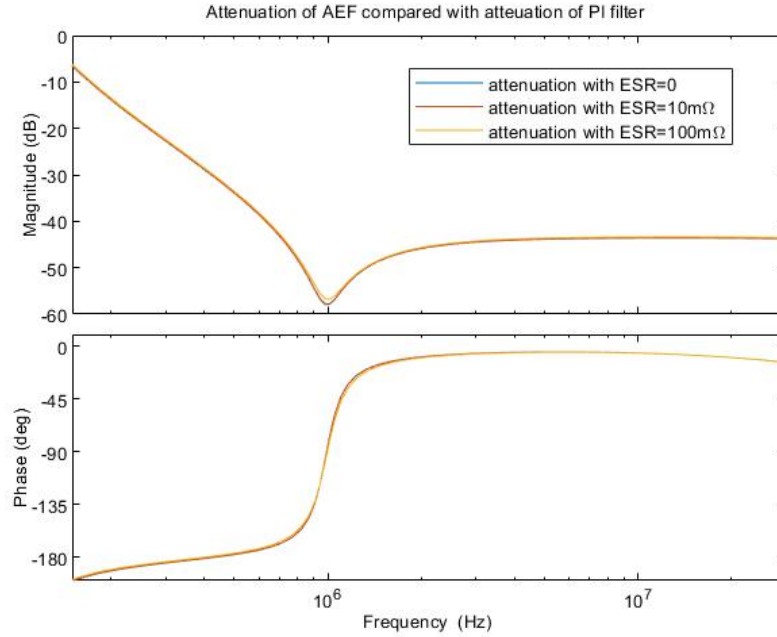


Figure 5.29: Comparison between attenuation of AEF with variation of ESR of $C_{INJ}, C_{SEN}, C_{AEFC}$.

A different type of approach in the design of the active filter consist in choosing a smaller value of inductor with respect to the passive solution. This determine an increase on the value of the capacitance that would be present in place of the AEF. But if the operational amplifier has a sufficient gain, the enhancement of the smaller capacitor of the active filter can be performed, obtaining a reduction in total area and volume.

The possibility to use a lower filter inductance value involves a physically smaller inductor that typically has a winding geometry with a lower parasitic winding capacitance and higher self-resonant frequency, leading to better filtering performance in the higher conducted frequency range.

Active EMI filtering (AEF) technology faces the two major challenges: to attenuate EMI guaranteeing a satisfactory attenuation level of the conducted emitted disturbances and to achieve a significant reduction in filter size and cost, along with improved performance.

Chapter 6

Conclusions

In conclusion a study on the electromagnetic compatibility of a DC/DC power converter provided by STMicroelectronics switching at a frequency of 1MHz is performed, computing and simulating the EMI conducted emissions. Considering the regulations, a simulation environment is set and the device is configured with the purpose of comparing the obtained emission value with the limits imposed by the international committee. According to EMC requirements, the equipment under test (EUT) must be tested at the rated voltage and under conditions which causes maximum disturbance. The studied device, that in normal operations works with an input voltage between 2.8V and 5.5V and an output voltage between 0.6V and 3.9V, is tested in worst condition for conducted emission with an input voltage of 5.5V and a duty cycle of 50%, with the maximum allowable load current, that is equal to 6A.

Having ascertained that the obtained conducted emissions exceed the required value, actions to mitigate these emissions level are mandatory, in order to obtain a compliant value even in the worst condition tested.

To mitigate the device's EMI a passive filter solution has been implemented, performing a study on the impact of the filter on the final system in which it is inserted. Analyzing how the dynamic performance are modified and examining the techniques used to ensure stability of the whole system. Taking into account these assessments and the required emission levels that must be respected to comply with the regulatory requirements, two different topologies of passive filters have been implemented: the LC filter and the π -type. Comparisons showed that a smaller size and volume of the selected components are obtained for the π -filter with respect to the LC one. Nevertheless, also in this case it has been obtained that the passive solution occupies a big portion of the total converter size, leading to a significant increase both in price and in board area.

Therefore, the active EMI filters technique based on the injection of signals with equal amplitude and opposite phase has been investigated. The unwanted interference signal is indeed measured and simultaneously canceled out by an antiphase copy of it, with the aim of completely removing it out or, at least, reducing it. The design phase has been tackled taking into account the required emission levels that must be respected and the consideration on the impact of the filter on the whole system's dynamic. Starting from the π -type filter topology, the active solution has been implemented using the same value of inductor of the π -filter and hence obtaining the same behaviour of the π -filter capacitor in the range of frequency of interest, but with smaller components. A non-negligible decrease in terms of total filter occupied area and costs was achieved: the reduction in size obtained is of the order of 50%, while the reduction in volume is of the order of 70%, instead as regards cost the reached reduction is about 75%. The active EMI filter technique further allows to obtain improved performance. This is due to the fact that in the π -filter even a small value of the capacitor's parasitic series resistance (ESR) is needed, as its value determines a significant variation in the value of attenuation and lead into a choice of bigger component to achieve the same reduction of disturbance. Furthermore, in the case of AEF there is the possibility to use a smaller inductor, with a winding geometry that has typically a lower parasitic winding capacitance and higher self-resonant frequency, which determines better filtering performance in the higher conducted frequency range.

Consequently, it can be stated that active EMI filtering technology faces the two major challenges: to attenuate EMI guaranteeing a satisfactory attenuation level of the conducted emitted disturbances and to achieve a significant reduction in filter size and cost.

Bibliography

- [1] CISPR 16-2-1:2014+AMD1:2017 CSV
- [2] Timothy Hegarty, *Noise Propagation And Filtering*. How2Power Today, Texas Instruments, Phoenix, Ariz (2018)
- [3] Timothy Hegarty, *An overview of conducted EMI specifications for power supplies*. Texas Instruments (2018)
- [4] CISPR 25:2021
- [5] CISPR 32:2015+AMD1:2019 CSV
- [6] CISPR 11:2015+AMD1:2016+AMD2:2019 CSV
- [7] Clayton R. Paul. *Introduction to Electromagnetic Compatibility*. John Wiley Sons, Inc., Second Edition (2006)
- [8] Petre-Marian Nicolae, Marius Voinea, *Modeling and Simulation of Electromagnetic Conducted Emissions from Buck Converter with Resistive Load*. IEEE University of Craiova/Electrical Engineering and Aeronautics Department (2012)
- [9] Andrei-Marius Silaghi, Ciprian Bleoju, Florin Berinde, Aldo De Sabata, *EMC Simulation of Conducted Emissions Produced by a DC-DC converter*. IEEE 26th International Symposium for Design and Technology in Electronic Packaging (SIITME) (2020)
- [10] Mikael Foissac, Jean-Luc Schanen, Christian Vollaire, *"Black Box" EMC model for Power Electronics Converter*. IEEE 978-1-4244-2893 (2009)

- [11] A. Ales, F. Tahar Belkacem and D. Moussaou, *Laboratory Line Impedance Stabilisation Network*. IEEE Electromagnetic Systems Laboratory Polytechnic Military School, EMP (2011)
- [12] Chuan Ni and Tateishi Tetsuo, *Adaptive Constant On-Time Control Study in Notebook Applications*. Application Report, Texas Instruments (2007)
- [13] CISPR 16-1-1:2019
- [14] Neal Zhang, Daniel Li, Vincent Zhang, Andy Chen, *Reduce Conducted EMI in Automotive Buck Converter Applications*. Application Report, Texas Instruments (2019)
- [15] Timothy Hegarty, *Predicting The Differential-Mode Conducted Noise Spectrum*. How2Power Today, Texas Instruments, Phoenix, Ariz (2020)
- [16] Le Yang, Shuo Wang, Hui Zhao, Yongjian Zhi, *Prediction and Analysis of EMI Spectrum Based on the Operating Principle of EMC Spectrum Analyzers*. IEEE Transactions on power electronics, VOL. 35, NO. 1, (2020)
- [17] Alan Martin, *AN-2162 Simple Success With Conducted EMI From DC-DC Converters*. Application Report, Texas Instruments (2013)
- [18] D.M. Mitchell, *Power line filter design considerations for DC-DC converters*. IEEE Industry Applicofionr Mogazine (1999)
- [19] Timothy Hegarty, *Input Filter Impact On Stability*. How2Power Today, Texas Instruments, Phoenix, Ariz (2019)
- [20] Zhang, Hao, *Simple Solution for Input Filter Stability Issue in DC/DC Converters*. Application Report, Texas Instruments (2019)
- [21] Robert W. Erickson Dragan Maksimovic, *Fundamentals of Power Electronics*. Kluwer Academic Publishers. Sixth Printing (2004)
- [22] Timothy Hegarty, *Differential Mode Input Filter Design*. How2Power Today, Texas Instruments, Phoenix, Ariz (2020)
- [23] Michele Sclocchi, *Input Filter Design for Switching Power Supplies*.

- National Semiconductor Corporation, Texas Instruments (2010)
- [24] Ali Shirsavar, *EMC Filter Design Part 5: Differential Mode Filter Damping Component Selection*. Biricha digital, technical videos (2019)
- [25] Christophe Basso – Technical Fellow IEEE Senior Member, *Input Filter Interactions with Switching Regulators*. ON Semiconductor (2017)
- [26] Timothy Hegarty, *Active And Hybrid Filter Circuits*. How2Power Today, Texas Instruments, Phoenix, Ariz (2021)
- [27] Balaji Narayanasamy and Fang Luo, *A Survey of Active EMI Filters for Conducted EMI Noise Reduction in Power Electronic Converters*. IEEE Transactions on electromagnetic compatibility, VOL. 61, NO. 6, (2019)
- [28] Orlando Murray, *How to reduce EMI and shrink power-supply size with an integrated active EMI filter*. Texas Instruments, technical article (2021)
- [29] Orlando Murray, *Using an Active EMI filter in power converters to reduce EMI filter size and cost*. India Automotive Seminar, Texas Instruments (2021)
- [30] *LM25149 42-V Synchronous Buck DC/DC Controller with Ultra-Low IQ and Integrated Active EMI Filter*. Texas Instruments (2021)